

**FOCUSING IN THE HOUGHTON
COLLEGE CYCLOTRON**

By

Sylvia I. Morrow

A thesis submitted in partial fulfillment of the
requirements for the degree of

Bachelor of Science

Houghton College

May 2015

Signature of Author.....

Department of Physics
May 11, 2015

.....

Dr. Mark Yuly
Professor of Physics
Research Supervisor

.....

Dr. Brandon Hoffman
Associate Professor of Physics

FOCUSING IN THE HOUGHTON COLLEGE CYCLOTRON

By

Sylvia I. Morrow

Submitted to the Department of Physics
on May 11, 2015 in partial fulfillment of the
requirement for the degree of
Bachelor of Science

Abstract

The small cyclotron at Houghton College loses most of its beam current to collisions with the Dee and chamber walls. The magnet is being altered to produce a more uniform increase in the radial magnetic field component with distance from the central plane. This will improve weak magnetic focusing as this component of the magnetic field creates a restoring force that pushes ions towards the central plane. Moreover, the field index value $n=0.2$ must not occur inside the maximum ion orbit radius to avoid coupled resonances. A computer model of the magnet and chamber was developed to test modifications of the magnet to achieve these results. A two dimensional cross-section of the magnet was modeled using Poisson Superfish, the results of which were used to track ions with the Simion 8.1 code. This model indicates a good chamber design is to replace the current aluminum chamber lids with magnetic stainless steel lids with radius 2.2 cm larger than the Dee. The steel lids direct the magnetic field lines radially outward, resulting in a more gradual change in field all the way to the outside edge of the Dee. This new design doubles the theoretical maximum kinetic energy to 900 keV for protons, but at these higher energies the ions fall out of phase before reaching the maximum radius because of the large number of orbits required. Results of the computer model will be compared with analytical results using a simplified model. Suggestions are made for future solutions.

Thesis Supervisor: Dr. Mark Yuly
Title: Professor of Physics

TABLE OF CONTENTS

Chapter 1: Introduction.....	2
1.1 Overview	2
1.1.1 History.....	2
1.1.2 Types of Accelerators.....	4
1.1.3 Modern Uses.....	5
1.2 Small Cyclotrons	6
1.2.1 Cyclotrino	7
1.2.2 Rutgers' Cyclotron	7
1.2.3 Cyclotron Kids	8
1.3 Motivation and Methods	8
Chapter 2: Theory	10
2.1 Principles of Cyclotron Operation.....	10
2.1.1 Basics	10
2.1.2 Electric Focusing.....	19
2.1.3 Weak Magnetic Focusing.....	20
2.1.4 Phase Shifting	22
2.1.5 Alternating Gradients.....	23
2.2 Model.....	24
2.2.1 Poisson Superfish.....	24
2.2.2 SIMION 8.1	24
Chapter 3: Analysis.....	27
3.1 Unmodified	28
3.2 Shims	37
3.3 Trim Coils.....	42
3.4 Chamber Lids.....	48
Chapter 4: Conclusion.....	54
4.1 Status and Future Plans	54
Appendix A: Poisson Superfish	56
A.1 Geometry File	56
A.2 PSF to SIMION	61
A.3 PSF General Analysis	62
Appendix B: SIMION 8.1	64

B.1	Rutgers Setup	64
B.2	Data Recording	65

TABLE OF FIGURES

Figure 1: A mechanical analog to the cyclotron.....	10
Figure 2: A basic cyclotron design.....	12
Figure 3: A cross-section of the cyclotron Dees showing the electric field lines inside the Dee gap.....	20
Figure 4: A cross-section of the magnet poles showing the magnetic field lines in the pole gap	22
Figure 5: A visual representation mesh points in a 3D SIMION potential array.....	25
Figure 6: Dee configuration in SIMION.	28
Figure 7: Schematic of the 2D representation of the unmodified cyclotron magnet.	29
Figure 8: A calibration for current density for PSF.....	30
Figure 9: An analysis the reliability of PSF calculations	31
Figure 10: PSF calculation of the magnetic field of the unmodified magnet.....	32
Figure 11: Magnetic field vs. radius in the central plane for the unmodified magnetic field.....	33
Figure 12: Field index vs. radius in the central plane for the unmodified magnetic field	34
Figure 13: Proton trajectory in the unmodified cyclotron magnetic field as calculated by SIMION.....	35
Figure 14: SIMION calculation of the axial position versus radius for the unmodified.....	35
Figure 15: An analysis of the frequency of axial oscillations about the central plane versus radius.	37
Figure 16: Schematic of the 2D representation of the shimmed cyclotron magnet.	38
Figure 17: PSF calculation of the magnetic field of the shimmed magnet	38
Figure 18: A comparison of the magnitude of the magnetic field vs. radius.....	39
Figure 19: A comparison of field index vs. radius.....	39
Figure 20: Proton trajectory in the SIMION calculation for the shimmed magnetic field	40
Figure 21: Axial position versus radius in the shimmed field according to SIMION calculations	40
Figure 22: Frequency of axial oscillations about the central plane versus radius for the shimmed	41
Figure 23: Trim coil geometry.....	43
Figure 24: Schematic of the 2D representation of the cyclotron magnet with trim coils.....	44
Figure 25: The current directions in adding and bucking trim coils.	45
Figure 26: Magnetic field strength versus radius for various configurations of trim coils.....	46
Figure 27: Magnetic field strength versus radius for various configurations of trim coils.....	47
Figure 28: Field index versus radius for various configurations of trim coils	48
Figure 29: PSF calculation of the magnetic field of the magnet with steel chamber lids.....	49
Figure 30: Magnitude of the magnetic field vs. radius	50
Figure 31: Comparison of the field index versus radius.....	50
Figure 32: Proton trajectory in the SIMION calculation for the steel lid magnetic field	51
Figure 33: Comparison of the vertical oscillations versus radius.....	51
Figure 34: The azimuthal position of the ion in the chamber.....	52
Figure 35: Angular phase difference versus radius for the steel lid magnetic field	53
Figure 36: Files and plot after Automesh execution.	60
Figure 37: Files and plot after Poisson execution.....	60
Figure 38: Interpolator window and files after interpolator execution.....	61

This project would like to acknowledge Dr. Timothy Koeth who generously made his model codes, instructional documents, potential array files, and personal insight available as a resource, invaluable accelerating the process.

Chapter 1

INTRODUCTION

1.1 **Overview**

1.1.1 History

In the 1930s, physicists began a focused effort to create machines that would allow them to accelerate ions to greater energies. The desire to accelerate ions was driven by the theorized ability to explore the structure of the nucleus, produce nuclear transmutations, and perform nuclear reactions using high energy nuclear collisions. As Ernest Lawrence, the creator of the first cyclotron said in his Nobel Lecture, “Rutherford and his school had clearly indicated that the next great frontier for the experimental physicist was surely the atomic nucleus” [1].

As is still the case even for contemporary accelerator designs, this was achieved by placing the ion in an electric field. Initial designs were as simple as placing a cold anode across from a hot metal cathode in a vacuum bulb which resulted in the production of x-rays from electrons bombarding the anode. However, the only way to increase the energy of the accelerated electrons in this design was to increase the potential difference applied. As physicists strove to accelerate a greater variety of particles to higher energies, they created new accelerator designs that avoided the engineering problem associated with insulating extremely high voltages [2].

Gustav Ising proposed the linear accelerator (linac) as a solution to the voltage problem by accelerating ions in a series of lower voltage steps [3]. However, as the accelerating tubes must pull the ions towards them initially and then push the ions away when the ion exits out the other side, the voltage on the accelerating tubes must alternate and oscillate. As the voltage on all accelerating tubes was designed to oscillate at the same frequency, it was necessary to systematically increase the length of accelerating tubes as the ion increased in energy and, therefore, velocity.

Lawrence borrowed Ising's idea of using successive voltage steps in his design for the cyclotron and, by using magnetic fields to keep ions moving in a circular path, Lawrence circumvented size problems that occur with the linac which must be longer and longer to reach higher energies while still using lower voltages. Like early accelerator designs, the cyclotron has only two electrodes; however, using radio-frequency (RF) voltages and magnetic fields, Lawrence designed the cyclotron so that the ions could be accelerated by these same electrodes many times. The magnetic field keeps the ions in a spiraling path, and the RF voltage assures that an ion won't be accelerated crossing the Dee gap one way just to lose all that energy when crossing in the other direction; rather, the Dee voltage is tuned to keep ions in phase. If the magnetic field is perfectly uniform throughout the entire vacuum chamber, the magnetic steering force increases in strength as the ion's velocity increases. The result is a spiraled path which naturally increases the particle path length with radius which also corresponds to increased particle energy. Lawrence discovered that in this system particles have the perfect ratio of increased velocity and increased path lengths to keep the period inside a Dee constant. This astonishing result allows the cyclotron to drive all particles at all radii simultaneously using constant frequency electrodes.

As Lawrence and his collaborators constructed multiple cyclotrons each with larger magnet pole faces in order to produce ions with higher energies and larger orbit radii, Sir John Cockcroft and Ernest Walton – still using the extremely high voltage accelerator design – recorded the first nuclear transmutation in an accelerator, producing two helium nuclei from a hydrogen-lithium collision. Lawrence and Livingston quickly followed their footsteps using their cyclotrons to perform similar experiments.

The kinetic energy of an ion in a cyclotron is proportional to both the magnet field squared and the ion radius squared, so a small increase in either of these variables results in a significant increase in ion energy. While in general either of these changes requires an increase in the size of a cyclotron, compared to the linac Lawrence's cyclotron design still minimized space requirements.

Cyclotron focusing techniques emerged out of a combination of theory and trial and error following the establishment of the basic cyclotron operation. While Lawrence's initial papers on the cyclotron

called for a “highly uniform magnetic field” [4], he later realized his magnetic field’s gradually increasing radial component, “surprising as it may seem, [was] an inhomogeneity that is really desirable” [1]. Lawrence found that the loss of resonance caused by the decrease in axial magnetic field was insignificant compared to the focusing the radial magnetic field component provided. This focusing technique is called weak magnetic focusing.

For modern accelerator beams, strong focusing using multipole magnets has become a common focusing technique. While originally developed by NC Christofilos in 1950 [5], Ernest Courant and Livingston independently developed and explored strong focusing techniques in 1952 [6]. While multipole magnets can be used in a cyclotron beam line after the beam has been extracted, strong focusing inside the cyclotron requires a thoughtfully designed azimuthal inhomogeneity which produces strong focusing effects.

With the success of the 60-inch cyclotron which increased the energy of the ions cyclotrons had been able to produce, Lawrence and his colleagues faced the quickly approaching question of how to handle the ion energies (around 25 MeV) that resulted in non-negligible increase in mass. This was problematic because cyclotron principles rely on constant mass to maintain resonance. While plausible cyclotron designs were proposed to confront this problem, ultimately more practical solutions for reaching higher energies emerged through mutations of the cyclotron such as the synchrocyclotron.

1.1.2 Types of Accelerators

The synchrocyclotron was created to increase the ion energy attainable from a cyclotron design. The basic design of the synchrocyclotron is identical to a standard cyclotron – when turned on it accelerates ions using constant frequency alternating voltage electrons. However, once ions in the chamber have reached relativistic energies, the RF frequency is slowly decreased. As a result, only a packet of ions that have just reached the relativistic barrier remain in resonance and continue to accelerate while all other ions in the chamber fall out of phase and begin to lose energy. The frequency is decreased at a rate which keeps the ion packet in phase so that its energy continues to increase.

Once the ion packet is extracted, this process is repeated. The result is a pulsed beam that reaches relativistic energies but with low intensity.

Modern accelerators tend to divide the steps of acceleration, focusing, and storage into separate components. The highest energy cyclic accelerator design is the synchrotron which uses this design. The synchrotron is torus-shaped tube into which pre-accelerated particles are injected. Before reaching the synchrotron, the ions are accelerated in a linac or a cyclotron. Typically the initial beam will be injected into a booster ring which utilizes a number of RF cavities around the ring to accelerate ions to relativistic speeds. The ions are only in the booster for a short time, however, before being injected into the synchrotron storage ring. This storage ring maintains the ion energy and is refilled by the linac-booster system as necessary. Synchrotrons are also useful because they are large enough to be fitted with multiple beamlines allowing the synchrotron to be used simultaneously for several different types of experiments with different ion extraction needs.

1.1.3 Modern Uses

The primary use of small cyclotrons in industry is for medical purposes. At low energies, the cyclotron is the ideal compact accelerator. For example, the University of Washington Medical Center has a small cyclotron that was initially installed to “treat cancer patients with fast neutron therapy” [7]. For over 30 years it has been used to conduct various types of radiotherapy both at the patient treatment and investigative research levels and to produce medical isotopes which are radioactive isotopes that doctors use to facilitate imaging or help target a specific organ with radiotherapy.

The National Superconducting Cyclotron Laboratory (NSCL) hosted at Michigan State University is the largest campus-based nuclear science facility in the country, currently operating two superconducting cyclotrons. Medical cyclotrons at NSCL are used to treat cancer patients, and the accelerator facilities are used to explore a wide range of nuclear research topics including exotic nuclei, rare isotopes [8], gamma spectroscopy, improved production of medical isotopes, nuclear astrophysics [9], accelerator physics [10], and more.

The TRI University Meson Facility (TRIUMF) facility at the University of British Columbia in Vancouver, British Columbia hosts the largest cyclotron in the world. Researchers at the TRIUMF facility cover many areas of research including nuclear medicine, materials science, nuclear structure, fundamental symmetries, and partner with international particle physics projects such as A Toroidal LHC ApparatuS (ATLAS) [11], [12].

1.2 Small Cyclotrons

Small cyclotrons have been built by a wide range of people from high-school students at El Cerrito to research scientists pursuing nuclear medicine. Most small cyclotrons mimic the early designs of Lawrence and Livingston, and many small cyclotron projects are built but then used infrequently. However, a few projects such as the Rutgers cyclotron and Houghton cyclotron are ongoing and used for educational purposes. These projects are engaged in the process of exploring small cyclotron dynamics and operations.

Houghton College students have worked for several years on the construction and operation of a mini-cyclotron with the goal of eventually conducting low-energy nuclear physics experiments with the beam produced [13]. The cyclotron features a Dee with a 3-inch radius and a corresponding dummy (grounded) Dee. These are placed in a vacuum chamber which is pumped down to around 10^{-6} Torr before being filled with a low pressure gas for ionization. The Houghton cyclotron produces ions using a filament which sits between the Dees at a floating voltage [14]. This causes electrons to be ejected off the filament, some of which end up between the Dees where they are affected by the electric and magnetic fields present. This results in a column of spiraling electrons which can ionize the hydrogen atoms present in the chamber. This process does not control the initial velocity of the resulting ion, so focusing considerations are essential for the Houghton cyclotron.

Other individuals and groups, described below, have built similar small cyclotrons for various purposes.

1.2.1 *Cyclotrino*

In 1987, J. J. Welch published [15] results from a small cyclotron called the cyclotrino developed at Berkley National Laboratory for the purpose of low energy studies, primarily for use as a mass spectrometer to separate ^{14}C from ^{12}C and ^{13}C for carbon dating techniques. The cyclotrino was particularly useful for samples where the percentage of ^{14}C present was so small that count rate dating techniques were ineffective. For this purpose, the cyclotrino was designed to provide a high resolution extraction window that could distinguish the small difference in mass between ^{14}C and its nearby isotopes or other contaminants such as hydrocarbons.

The cyclotrino, extracting its beam at a 10 cm radius, was very similar in size to the Houghton College cyclotron. However, it had certain unique features in order to facilitate its use as a mass spectrometer. While all cyclotrons can operate at odd harmonics of the resonant frequency, for most cyclotrons running at higher frequencies is counterproductive as it can result in decreased beam intensity because ions fall out of phase sooner – a feature the cyclotrino took advantage of to increase mass spectroscopy resolution. Resonance frequency is dependent on ion mass, so the cyclotrino calculated its resonant frequency using the mass of ^{14}C . For a standard cyclotron, ^{12}C and ^{13}C are close enough in mass to ^{14}C that this frequency is close enough to their resonant frequency that they would often make it out to the extraction radius without falling completely out of phase. The cyclotrino uses high harmonics to accelerate the process of falling out of phase so that unless the ion is the exact mass selected for, it is likely to fall out of phase before reaching the outer edge, leaving only the isotope selected for at the collector. The cyclotrino operated up to the 15th harmonic which means the Dees went through their voltage cycle seven times in the time it took an ion to complete the semi-circular path through a Dee. This technique for achieving high resolution is dependent on an extremely controlled and precise phase. As such, weak magnetic focusing techniques (which necessitate some variation in phase) were unusable.

1.2.2 *Rutgers' Cyclotron*

Timothy Koeth and Stuart Hanebuth built a 9-inch mini-cyclotron at Rutgers University in the late 1990s [16]. Since then Koeth and collaborators have conducted extensive testing of the cyclotron and

upgraded to a 12-inch cyclotron with plans to further upgrade to a 19.5-inch cyclotron. The Rutgers cyclotron is used as an educational tool for undergraduate students. A phosphor screen may be placed inside the cyclotron in the place of a current collector, creating a visible beam that is useful for diagnostics. The Rutgers cyclotron initially used a filament ion source before upgrading to a chimney ion source and more recently upgrading to a PIG source [17], 18. The Rutgers cyclotron is a rich resource for mini-cyclotron operators as it has been tested with a wide range of cyclotron components including various pole tip designs to test their focusing capabilities. To the significant benefit of this project, the successful computer model of the Rutgers cyclotron was used as a foundation for the model of the Houghton cyclotron.

1.2.3 Cyclotron Kids

In 2006, high school students Heidi Baumgartner and Peter Heuer, with support from Jefferson National Laboratory, constructed a cyclotron with 6-inch radius Dees and a theoretical maximum kinetic energy of 2.85 MeV for protons [19]. In order to reduce the total path length, they used a Dee voltage of 10kV peak-to-peak. Baumgartner and Heuer planned for the focusing needs of their cyclotron by using pole tips that implemented a 0.02 inch convex taper. This design bends the magnetic field lines and alters the shape of the magnetic field between the poles in such a way that aids weak focusing.

1.3 Motivation and Methods

The range of nuclear experiments which could be performed with the Houghton cyclotron could be significantly increased if it were able to accelerate ions to around 1 MeV. The theoretical maximum kinetic energy of the current design is around 0.5 MeV for protons, but in practice the cyclotron has so far accelerated ions to only around 10-100 keV. The goal of this project was to model the cyclotron in an attempt to understand why the current design is not reaching the theoretical maximum energies, and to propose design modifications that would solve this problem and increase the theoretical maximum of the design.

The effects of thin sheets of iron, called shims, on the magnetic field were studied in an attempt to improve focusing. This common method of altering the magnetic field shape was determined to be impractical for Houghton's mini-cyclotron. The impact of bunched trim coils with varied currents and in various arrangements was studied. This method showed potential but was superseded by a simpler, more effective design: replacing the vacuum chamber lids with magnetic steel plates. As the radius of the chamber is greater than that of the poles, using magnetic steel lids created an effective increase in pole radius. This design also reduced the effective pole gap which increased the magnetic field strength resulting in an increase in theoretical maximum kinetic energy of the cyclotron to 0.9 MeV for protons. Furthermore, this design improved the linearity of the field with radius which benefits weak focusing.

The model calculations have provided new insight into the cyclotron's apparent inability to reach the design's theoretical maximum. The calculations suggest that defocusing effects are smaller than was initially assumed, but that phase shifting is a larger problem than was anticipated. Further studies are being considered to solve this issue.

The method of modelling the cyclotron was chosen as a long-term investment. Now that the model has been made, it can easily be adapted to predict the consequences of potential future design adaptations. The specific modeling software was chosen because it had already been successfully used to model the Rutgers cyclotron.

Chapter 2

THEORY

2.1 Principles of Cyclotron Operation

Cyclotron theory emerges from a combination of electromagnetic theory and theory of circular motion, yet the principles that govern the basic principles of cyclotron motion are deceptively simple.

2.1.1 Basics

The method of cyclotron acceleration is easily conceptualized via a mechanical analog seen in Figure 1. Two semicircular plates with spiraled grooves milled into them at various radii can be oscillated up and down. The frequency of this oscillation can be set such that if a ball begins on the elevated plate at the center of the circle, every time it reaches the center line that divides the plates, it is sitting on an elevated plate and will, therefore, fall down the gap resulting in increased kinetic energy. If ball fell back into the same groove, it would complete the semi-circular path quicker than it did the first time, and it would approach the plate gap before the plates are in the correct position.

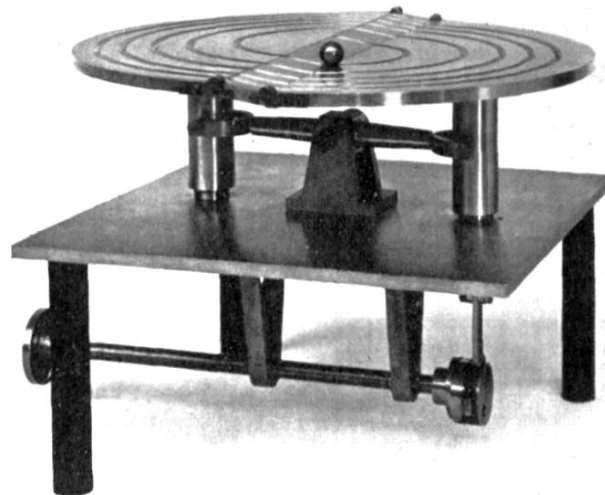


Figure 1: A mechanical analog to the cyclotron. Figure from Ref. [20]

As such, the ball must fall into a groove with a larger radius to increase the path length in such a way that is proportional to the increase in velocity so that the ion period on a play remains constant. As long as this resonance between the ball and the frequency of the plate oscillations is maintained, the ball will continue to gain energy and the ball will need to move out to increasing radii until it reaches the limits of the edges of the plates at which point it is extracted.

The goal of a cyclotron is to accelerate ions using a series of low voltage steps. The cyclotron achieves this with the help of the “resonance principle” [21]. As in the mechanical analog described, a cyclotron has two Dees with varying potential; however, for an actual cyclotron the Dees are hollow, semicircular electrodes placed across from each other in an evacuated chamber with a small gap between them, as shown in Figure 2. Analogous to how the ball of the mechanical analog gains kinetic energy from the gravitational potential energy when it falls from the elevated to the lowered Dee, the ions in a cyclotron chamber gain kinetic energy by crossing the electrical potential between the different Dees. Ions generated between the Dees in the center of the vacuum chamber are accelerated by the electric field between the Dees until they are inside the Dee which, being a nearly enclosed structure made of a conducting material, is an approximately electric-field-free region.

The vacuum chamber containing the Dees is placed between two magnet poles resulting in a nearly uniform magnetic field throughout the chamber. The resulting force on the ion moves it in the circular path imitated by the grooves in the mechanical analog. Inside the Dees the primary force on the ions is the magnetic field component of the Lorentz force,

$$\vec{F} = q(\vec{E} + \vec{v} \times \vec{B}) \quad (1)$$

where \vec{F} is the Lorentz force, q is the charge of the ion, \vec{E} is the electric field, \vec{v} is the ion velocity, and \vec{B} is the magnetic field. As the magnetic field is orthogonal to the plane of the chamber (which is considered the axial direction) and the ion velocity is primarily in the azimuthal direction, the resulting force is radial which is what keeps the ion moving in its spiral path.

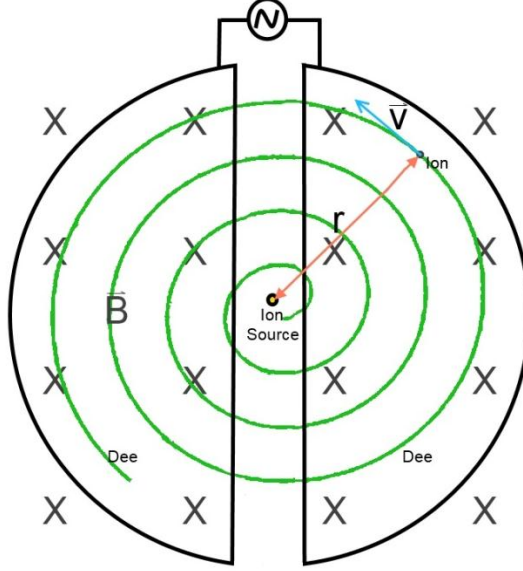


Figure 2: A basic cyclotron design. Two Dee shaped electrodes are connected to an RF voltage source. An ion source is between these electrodes. A uniform magnetic field pointed into the page fills the chamber.

For cyclotrons it is helpful to express this equation in cylindrical coordinates. Since, in cylindrical coordinates, the acceleration \vec{a} is

$$\vec{a} = (\ddot{r} - r\dot{\theta}^2)\hat{r} + (2\dot{r}\dot{\theta} + r\ddot{\theta})\hat{\theta} + \ddot{z}\hat{k}, \quad (2)$$

then under the assumption that mass is constant which is reasonable for the Houghton cyclotron which does not get near relativistic energies, Eq. 1 can be written as

$$m\{(\ddot{r} - r\dot{\theta}^2)\hat{r} + (2\dot{r}\dot{\theta} + r\ddot{\theta})\hat{\theta} + \ddot{z}\hat{k}\} = q\{(E_r + r\dot{\theta}B_z - \dot{z}B_\theta)\hat{r} + (E_\theta + \dot{z}B_r - \dot{r}B_z)\hat{\theta} + (E_z + \dot{r}B_\theta - r\dot{\theta}B_r)\hat{k}\} \quad (3)$$

which can be separated into three component equations.

One way to express the axial component of the magnetic field, B_z is in terms of a constant called the field index, n

$$B_z = B_0 \left(\frac{r_0}{r}\right)^n \quad (4)$$

which can then be used to calculate the specific conditions necessary to achieve orbital stability [22]. This field is described in terms of r_0 , the radius of some equilibrium orbit from which, in the period considered, the ion only makes small variations and B_0 which is the axial component of the magnetic field at that radius. As will be justified by Eq. 30, the field index must be a positive. To solve for the field index, take the derivative of Eq. 4 with respect to r

$$\frac{dB_z}{dr} = B_0 r_0^n (-n) r^{-n-1} \quad (5)$$

and solve for n ,

$$n = -\frac{r}{B_z} \frac{dB_z}{dr}. \quad (6)$$

To solve for the conditions of orbital stability, consider a Taylor expansion of part of Eq. 4 around r_0

$$\left(\frac{r_0}{r}\right)^n = \left(\frac{r_0}{r_0}\right)^n + (r - r_0)[r_0^n (-n) r^{-n-1}]_{r=r_0} + \dots \quad (7)$$

which yields, to first order in $\frac{\Delta r}{r_0} \ll 1$,

$$\left(\frac{r_0}{r}\right)^n \approx 1 - \frac{n\Delta r}{r_0} \quad (8)$$

where $\Delta r = r - r_0$. Therefore, Eq. 4 can be approximated as

$$B_z \approx B_0 \left(1 - \frac{n\Delta r}{r_0}\right). \quad (9)$$

The radial component of the magnetic field can be found using Ampere's law in vacuum,

$$\nabla \times \vec{B} = \mu_0 \vec{J} + \mu_0 \epsilon_0 \frac{\partial \vec{E}}{\partial t} \quad (10)$$

the right-hand side of which equals zero inside the Dee. Therefore, in the case of an

azimuthally uniform field where $\frac{\partial B_z}{\partial \theta} = \frac{\partial B_r}{\partial \theta} = B_\theta = 0$,

$$\nabla \times \vec{B} = \hat{r} \left(\frac{\partial B_z}{\partial \theta} - \frac{\partial r B_\theta}{\partial z} \right) - \hat{\theta} \left(\frac{\partial B_z}{\partial r} - \frac{\partial B_r}{\partial z} \right) + \frac{\hat{k}}{r} \left(\frac{\partial r B_\theta}{\partial r} - \frac{\partial B_r}{\partial \theta} \right) = \hat{\theta} \left(\frac{\partial B_z}{\partial r} - \frac{\partial B_r}{\partial z} \right) = 0 \quad (11)$$

such that,

$$\frac{\partial B_r}{\partial z} = \frac{\partial B_z}{\partial r}. \quad (12)$$

This relationship is key for weak magnetic focusing. To find the equations of motion for the particle in this field, Eq. 9 and Eq. 12 can be combined to yield

$$\frac{\partial B_r}{\partial z} = -\frac{nB_0}{r_0}. \quad (13)$$

Assuming $B_r = 0$ at $z = 0$, integration yields

$$B_r = -\frac{nB_0}{r_0}z. \quad (14)$$

The axial (\hat{k}) component of Eq. 3 is

$$m\ddot{z} = q(E_z + \dot{r}B_\theta - r\dot{\theta}B_r) \quad (15)$$

where $E_z = 0$ inside the Dee and $B_\theta = 0$ for this magnetic field in general. Substituting in Eq. 14, and assuming velocity is given by $v = r\dot{\theta}$ yields

$$m\ddot{z} = qv\frac{nB_0}{r_0}z. \quad (16)$$

The radial (\hat{r}) component of Eq. 3,

$$m(\ddot{r} - r\dot{\theta}^2) = q(E_r + r\dot{\theta}B_z - \dot{z}B_\theta), \quad (17)$$

where $E_r = 0$ inside the Dee and $B_\theta = 0$ still equals zero, can be expressed as

$$m\left(\ddot{r} - \frac{v^2}{r}\right) = q\left[vB_0\left(1 - \frac{n\Delta r}{r_0}\right)\right] \quad (18)$$

by substituting in Eq. 9 and assuming $v = r\dot{\theta}$. As $\Delta r = r - r_0$ where r_0 is a constant,

$$m\frac{d^2r}{dt^2} = m\frac{d^2}{dt^2}(\Delta r + r_0) = m\frac{d^2\Delta r}{dt^2}. \quad (19)$$

Furthermore, using a first-order approximation of a binomial expansion

$$\frac{1}{r} = \frac{1}{\Delta r + r_0} = \frac{1}{r_0} * \frac{1}{1 + \frac{\Delta r}{r_0}} = \frac{1}{r_0}\left(1 + \frac{\Delta r}{r_0}\right)^{-1} \approx \frac{1}{r_0}\left(1 - \frac{\Delta r}{r_0}\right) \quad (20)$$

such that Eq. 18 can be written as

$$m \left[\frac{d^2 \Delta r}{dt^2} - \frac{v^2}{r_0} \left(1 - \frac{\Delta r}{r_0} \right) \right] = qvB_0 \left(1 - \frac{n\Delta r}{r_0} \right). \quad (21)$$

Since the equilibrium orbit has been defined such that the ion only makes very small

excursions from r_0 , if we require $\Delta r \approx \frac{d^2 \Delta r}{dt^2} \approx 0$ Eq. 21 becomes

$$-\frac{mv^2}{r_0} = qvB_0 \quad (22)$$

which is the standard cyclotron orbit equation in a uniform field. Notice the right side of this equation is the centripetal force which must be equal and opposite to the Lorentz force on the ion at the same radius. Substituting the angular velocity $\omega_0 = \frac{v}{r_0}$ into Eq. 16 and Eq. 21 puts these equations into the

form of equations of motion:

$$m\ddot{z} = -m\omega_0^2 nz \quad (23)$$

and

$$m\Delta\ddot{r} = m \frac{v^2}{r_0} \left(1 - \frac{\Delta r}{r_0} \right) + \left(-\frac{mv^2}{r_0} \right) \left(1 - \frac{n\Delta r}{r_0} \right) \quad (24)$$

which becomes

$$\ddot{z} = -\omega_0^2 nz \quad (25)$$

and

$$\Delta\ddot{r} = -\omega_0^2 \Delta r (1 - n). \quad (26)$$

It is useful for an analysis of focusing to also understand the ion's motion in terms of the frequency of its axial and radial oscillations about the equilibrium orbit. The general form of a harmonic oscillator equation of motion is

$$\frac{d}{dt} \dot{x} = -\omega_0^2 x \quad (27)$$

where ω_0 is the natural frequency of oscillation. Inspection of Eq. 23 and Eq. 26 shows that the frequency of oscillation in the z and r directions is given, therefore, by

$$-\omega_r^2 \Delta r = -\omega_0^2 (1 - n) \Delta r \quad (28)$$

and

$$-\omega_z^2 z = -\omega_0^2 n z. \quad (29)$$

or

$$\omega_r = \omega_0 \sqrt{1 - n} \quad (30)$$

and

$$\omega_z = \omega_0 \sqrt{n}. \quad (31)$$

Notice Eq. 30 and Eq. 31 justify the requirement that the field must satisfy $0 \leq n \leq 1$ for regular cyclotron motion because these are the only values of n that give a real solution for angular velocity. As n increases with r , ω_z also increase with r ; therefore, as Eq. 25 and Eq. 26 are proportional to ω^2 , this indicates that the amplitude of ion oscillations will decrease with time.

Recall $f = \frac{\omega}{2\pi}$, so if both sides of Eq. 30 and Eq. 31 are divided by 2π , the frequency is obtained,

$$f_r = f_0 \sqrt{1 - n} \quad (32)$$

and

$$f_z = f_0 \sqrt{n} \quad (33)$$

where f_0 is the resonance frequency which is the frequency in a uniform field. The oscillations described by these equations are called “free oscillations” or betatron oscillations.

To determine the value of f_0 , consider the idealized cyclotron model depicted in Figure 2 where the ion velocity is always orthogonal to the uniform magnetic field in this system and inside the Dees is effectively an electric field-free region. In this case, Eq. 22 justifies a simplified approximation of the equations of motion that describes the radial force on the ion as

$$-F_r = \frac{mv^2}{r} = qvB_z \quad (34)$$

where m is the ion mass, r is the ion’s radial position, and B_z is the axial component of the magnetic

field, which under the assumption that the field is uniformly axial, is all of B . This simplifies to,

$$\frac{v}{r} = \frac{qB_z}{m}. \quad (35)$$

This means the cyclotron frequency, f_0 , can be written as,

$$f_0 = \frac{\omega_0}{2\pi} = \frac{1}{2\pi} \frac{v}{r} = \frac{qB_z}{2\pi m}. \quad (36)$$

This amazing independence of ion frequency and ion radius is essential for the concept of the fixed frequency cyclotron to work. It means a particular resonance frequency f_0 can be determined for a given ion and cyclotron geometry with a magnetic field of B_z , and the cyclotron is able to drive all ions at all radii simultaneously using constant frequency electrodes.

Note that while Eq. 36 is the frequency required to achieve half a voltage cycle during the time the ion moves through a Dee, odd multiples of this frequency will also work. For example, for Dees set to a resonance frequency of $3f$, the Dee voltage would go through one and a half cycles while the ion moves through the Dee, and the Dee voltage would still be at the optimal point in the voltage cycle when the ion returns to the Dee gap.

Solving for ion velocity in Eq. 35, the kinetic energy, T , of ions will be

$$T = \frac{1}{2}mv^2 = \frac{1}{2}m\left(\frac{qB_z r}{m}\right)^2 = \frac{(qB_z r)^2}{2m} \quad (37)$$

where maximum kinetic energy occurs for ions at the maximum achievable radius, the Dee radius, which for the Houghton cyclotron is 7.8 cm. Ions in resonance gain energy equal to the potential difference between the Dees each time they cross the gap.

Rearranging Eq. 37 for r yields

$$r = \frac{\sqrt{2mT}}{qB_z} \quad (38)$$

which means, going from a radius r_1 with kinetic energy T_1 to radius r_2 with kinetic energy T_2 , the

change in radius, $\Delta r = r_2 - r_1$, is

$$\Delta r = \frac{\sqrt{2m}}{qB_z}(\sqrt{T_2} - \sqrt{T_1}), \quad (39)$$

but as the kinetic energy always increases for a full orbit (which requires that the ion cross the Dee gap twice) by the constant $\Delta T = 2e\Delta V$,

$$\Delta r = \frac{\sqrt{2m}}{qB_z}(\sqrt{T_1 + 2e\Delta V} - \sqrt{T_1}) \quad (40)$$

where V is the potential across the gap. As T_1 increases, the expression in the brackets decreases in magnitude, and since the expression outside of the brackets is constant, Δr also decreases. Therefore, while Eq. 38 indicates that an increase in kinetic energy increases the radius of an ion's path, the Δr increase in ion radius will decrease as the kinetic energy of the ion increases.

The number of beam revolutions required to reach maximum energy can be found by dividing maximum kinetic energy by double the energy gained by an ion each time it crosses the Dee gap which equals the amplitude of the Dee voltage:

$$N = \frac{T}{2e\Delta V}. \quad (41)$$

For an ideal model, the number of times an ion spirals around the chamber will not matter except that it increases the time taken for the ion to reach its maximum kinetic energy. However, in a real cyclotron, most ion velocities are perturbed in the axial direction when they are produced at the source, even in ion source designs that attempt to control the ion's initial velocity. Therefore, unless N is so small that ion path is extremely short, cyclotrons require focusing to keep ions near the central plane as they move through the chamber.

Methods of weak (and some strong) focusing require a radial component of B_r (and an azimuthal component B_θ or for strong focusing), which means B_z changes with radius. However, Lawrence noted that synchronization is possible even when the axial component of the magnetic field decreases in strength, changing the resonance frequency, Eq. 36, as long as the Dee voltage is high enough (or

the desired kinetic energy is low enough) that the ions do not have to make so many revolutions that this change in resonance seriously affects their phase.

2.1.2 *Electric Focusing*

Restoring forces caused by the shape of the electric field in the cyclotron can produce a focusing effect. Because of the electrode configuration, the electric field is small except for near the Dee gap, so electric focusing can only take place near the Dee gap. Generally speaking, the energy gained by this force is small enough that it is only significant compared to ion kinetic energy in the initial stage when the ion is still at a low energy. However, in these initial stages of the ion's motion as it first begins to orbit, electric focusing can help keep the ion near the central plane. Robert Wilson quantified the effect of electric focusing using analytical calculations and found that minimizing the ratio $\frac{d}{h}$, where d is the Dee gap and h is the Dee height, maximizes focusing [23]. For the Houghton cyclotron, $\frac{d}{h} \approx 0.6$.

As a result of the shape of the electric field as seen in Figure 3, the ion experiences both electric focusing and defocusing every time it crosses the Dee gap. When in phase, the Dee gap acts as an accelerating lens.

Consider the ion trajectory (solid line) on the upper half of Figure 3. This ion approaches the Dee gap defocused, moving upwards away from the central plane. Considering only forces caused by the electric field, as the ion enters the Dee gap it experiences a force downwards and to the right, focusing it and accelerating it across the gap. Once the ion crosses the center of the Dee gap, the forces on it are upwards and to the right. However, because the ion is closer to the central plane than it was as it crossed the first half, the relative magnitude of the upwards force is smaller than the downwards force was, and the magnitude of the force to the right increases. The force to the right continues to accelerate the ion across the gap, and the upwards force starts to defocus the ion, pushing it away from the central plane. However, because the magnitude of the upwards defocusing force is smaller than

that of the downwards focusing force and because the ion spends less time in the second half of the gap (because it continues to be accelerated to the right), the defocusing force does not change the ion path as much as the focusing force did, so the net effect is focusing, and the ion leaves the Dee gap at an angle to the central plane that is smaller than the angle at which it entered. The same principle would apply to the ion trajectory drawn in the bottom half of Figure 3.

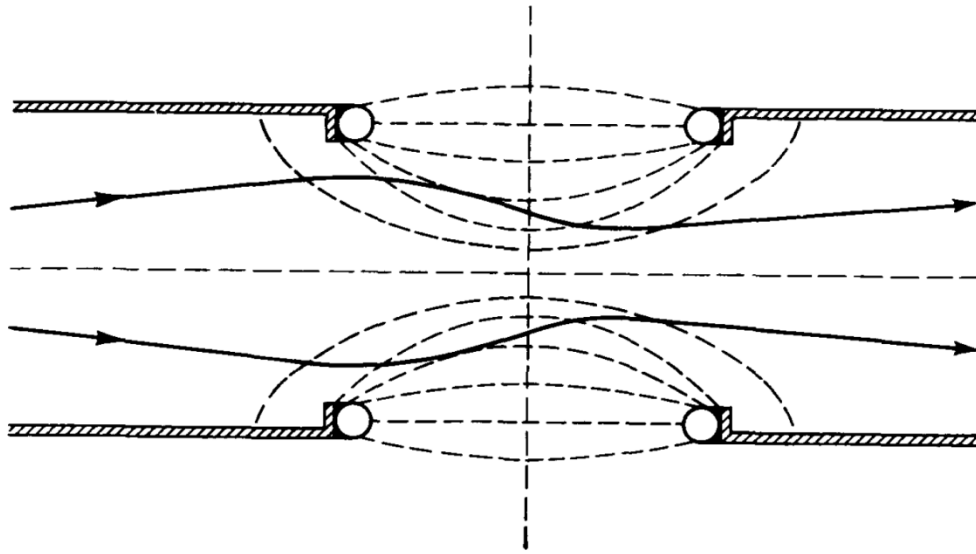


Figure 3: A cross-section of the cyclotron Dees showing the electric field lines inside the Dee gap (dashed lines) and an exaggerated depiction of the ion path (solid line) through that region. Figure taken from Ref [24].

Wilson’s analysis of electric focusing in cyclotrons concluded that it is “negligible at large path radii” which for the example he considered was at radii at least one third of the way into the chamber.

2.1.3 *Weak Magnetic Focusing*

Weak magnetic focusing occurs in the cyclotron Dees and produces a restoring force that pushes ions towards the central plane. This is necessary for cyclotron focusing as it causes ions oscillate around the central plane which prevents them from colliding with the Dee walls. While, as discussed in Section 2.1.1, the uniformity of the magnetic field is essential for maintaining cyclotron resonance, it turns out

that weak magnetic focusing requires a radial magnetic field component which requires a changing magnetic field.

The relationship between B_z and B_r established in Eq. 12 is essential for determining the ideal field shape for weak magnetic focusing. The goal of focusing in general is to keep the ions close to the central plane. Weak magnetic focusing does this by letting the B_r increase in strength as the axial distance from the central plane increases resulting in a corresponding stronger focusing force. Eq. 12 indicates that controlling the rate at which B_z changes with radius will indirectly provide control over B_r . A simple option would be to design the magnetic field such that B_z decreases in strength linearly with radius. Considering Eq. 12, therefore,

$$\frac{\partial B_r}{\partial z} = \frac{\partial B_z}{\partial r} = C \quad (42)$$

where C is a constant equal to the slope of the linear decrease, and B_r will linearly increase in strength with distance from the central plane at the same rate. The relationship $B_r = Cz$ obtained from an integration of Eq. 42 indicates that ions in this field will experience simple harmonic motion around the central plane. Therefore, weak magnetic focusing can be achieved by producing a magnetic field in which B_z linearly decreases. That is, for the cyclotron magnet in cylindrical coordinates as shown in Figure 4, the Lorentz force, Eq. 1, on the ion is orthogonal to both the velocity and the magnetic field vector. As such, a radial component to the magnetic field (B_r) will add an axial component to the force which points towards the central plane (F_z).

Numerous methods have been attempted to achieve the ideal magnetic field shape. As part of his exploration of weak magnetic focusing, Lawrence used shimming to shape his magnetic field. Shimming involves the insertion of thin iron sheets (typically 0.25 inches or less) between the pole faces and the vacuum chamber. Lawrence used empirical determinations to position his shims and tweak the shape of his magnetic field. Many different shapes and sizes of shims have been used to facilitate the field-shaping needs of specific cyclotrons.

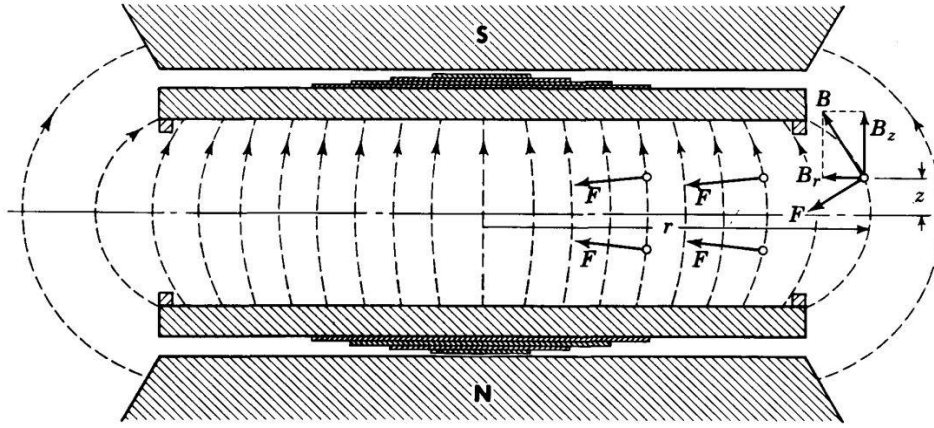


Figure 4: A cross-section of the magnet poles showing the magnetic field lines in the pole gap and the forces on ions in various positions. The velocity of the particles shown on the right-hand side points out of the page. Figure taken from Ref. [24].

2.1.4 Phase Shifting

The axial component of the magnetic field can be decreased at larger radii in order to increase the radial (focusing) component, provided the ions only have a few revolutions left once they reach this portion of the field. This can be achieved by increasing Dee voltage so that the ions gain more energy each time they cross the gap such that they require fewer revolutions overall to achieve their maximum energy. The consequence of crossing the gap many times when the ion and Dees are out of phase is called phase shifting.

Qualitatively, the problem with phase shifting is that if an ion enters the Dee gap slightly out of phase, the RF voltage will begin to switch polarity before it finishes crossing the gap. As a result, the ion gains less energy in this gap crossing. The more out of phase the ion becomes, the less energy it will gain when crossing the Dee gap and the more orbits it will require to reach maximum energy, thus exacerbating the phase shifting problem. Furthermore, once the phase shift becomes acute, the ion can fall completely out of phase at which point its energy does not change at all when crossing the gap. Beyond this point, the phase shift will continue to increase, however the ion will begin to approach the Dee gap when the voltage is at a point in its cycle that repels the ion from the opposite Dee and draws

it towards the Dee it is emerging from such that the ion kinetic energy actually decreases as it crosses the gap. This results in an ion trajectory that spirals back inward towards the center.

If many ions in the beam fall out of phase before reaching maximum Dee radius, the beam current will drop suddenly to near zero beyond whatever radius the ions tend to reach before falling so out of phase that they stop gaining energy.

Fundamentally the issue is the changing magnetic field. In a completely uniform field, ions would never fall out of phase. However, unless the ions were produced with the physically irreproducible initial condition of ion velocity only in the direction of the central plane, the only restoring force that might focus perturbed trajectories is the electric focusing which is quite weak. As such, in order to use weak magnetic focusing, it is necessary to strike a balance which allows the axial magnetic field to decrease when it is more beneficial to have focusing than it is problematic to have phase shifting. Reducing the number of revolutions required to reach maximum kinetic energy reduces phase shifting because it shortens the ion's total path length. Shorter path length is also desirable because it means that the ion spends less time in the chamber making it less likely for it to collide with residual gas particles in the chamber.

2.1.5 Alternating Gradients

Alternating gradient (AG) focusing, sometimes referred to as strong focusing, requires that a beam pass through adjacent orthogonal fields, accomplished for cyclotrons by using segmented or spiral pole tips [6]. AG focusing emerged as a response to problems with reaching relativistic energies in cyclotrons as it can be designed to increase the axial component of the magnetic field with radius in such a way that counters the increase in mass of ions as they reach relativistic energies. However, AG focusing is also ideal for the Houghton cyclotron even though it does not reach relativistic energies as the principles can be exploited in such a way that will produce a focused beam that avoids phase shifting problems. This is achieved by using strong focusing forces while also maintaining a constant average magnetic field strength to keep ions in phase.

One type of AG focusing, sector focusing, keeps ions in stable, axially oscillating orbits near the central plane using what is called the “Thomas” force. This restoring force occurs when an ion with a component of velocity in the radial direction goes through a magnetic field with an azimuthal component resulting in an axial force towards the central plane. This requires, however, a significantly different magnetic field than one designed to increase weak focusing which strives for azimuthal symmetry. Spiral pole tips have been shown to successfully increase the Thomas force while also using the radial component of the magnetic field, providing two interacting focusing forces.

2.2 Model

In order to tackle problems of defocusing and phase shifting in the Houghton cyclotron, two programs were used to model the cyclotron magnetic and electric fields and calculate an ion’s path. Poisson Superfish (PSF) was used to make a two dimensional model of the cyclotron magnet, and SIMION 8.1 was used to model the electric field between the Dees and calculate the ion path.

2.2.1 *Poisson Superfish*

PSF is a software package containing several interconnected programs that function as a finite element (FEM) field solver for 2D planar or cylindrical symmetries. The Automesh program uses a user-created geometry file to generate a mesh for use by Poisson or Pandira which solve for the magnetic field using a successive approximation method and a matrix diagonalization method respectively. This project used Poisson which calculates the magnetic field of a given geometry using successive point over-relaxation of Laplace’s equation for the magnetic potential,

$$\nabla^2 \phi = 0. \quad (43)$$

According to the PSF manual, “It calculates the derivatives of the potential, namely, the fields and their gradients, calculates the stored energy, and performs harmonic (multipole) analysis of the potential.” This solution can be viewed graphically using the Wsfplot program.

2.2.2 *SIMION 8.1*

A three-dimensional model of the cyclotron Dees, originally designed for the Rutgers’ cyclotron in the modelling software SIMION 8.1, was used to calculate ion paths in magnetic fields calculated by PSF.

SIMION, designed to solve electrostatic potentials and magnetic fields [25] solves the cyclotron model which has electrodes whose potentials change with time using iterating steps of electrostatic solutions. SIMION ignores the ions and solves for the electric field using Laplace's equation,

$$\nabla^2 V = 0 \quad (44)$$

which is true in empty space. In Cartesian coordinates this can be written as

$$\frac{\partial^2 V}{\partial x^2} + \frac{\partial^2 V}{\partial y^2} + \frac{\partial^2 V}{\partial z^2} = 0. \quad (45)$$

This requires that the derivative of the potential is constant in all directions, so the potential is changing at a constant rate. SIMION takes advantage of this with a finite difference technique called “over-relaxation” to estimate the potential at non-electron points by assuming that the potential at one point is approximately equal to the average of all the points around it.

As such, SIMION uses arrays to compute the potential. A packed array will have, at each coordinate point, information about the voltage at that point and whether or not it is an electrode. Successive iterations of the calculation take the average of the potentials of each point adjacent to every non-electrode point. For example, in Figure 5, the new potential of $p0$, the mesh point at the origin, would be $V0_{new} = (V1 + V2 + V3 + V4 + V5 + V6)/6$, the average of the potentials of all six adjacent mesh points.

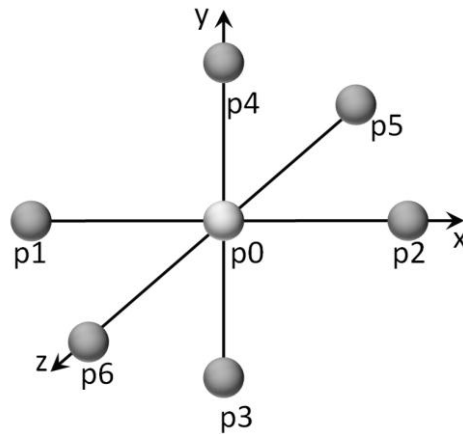


Figure 5: A visual representation mesh points in a 3D SIMION potential array. The point $p0$ has six adjacent potential points. The potential of all six are averaged to determine the potential at $p0$.

For an electrostatic field, the more iterations of the calculation performed, the less the values of the potential will change. When many iterations have been performed and any changes in the potential upon successive iterations is considered negligible compared to the degree of accuracy the user has set SIMION to solve for, the system is considered to be stabilized. In an electrodynamic field, however, the voltage of electrode points varies with successive iterations, so these changes are continuously propagated by the non-electrode points adjacent to electrode points. Over-relaxation speeds up the refining of this process.

An ion workbench is a user-created program which can be opened in SIMION and configured to access a set of potential arrays.

The variable *T.Qual*, the trajectory quality factor, determines the step distance of a calculation in “grid units.” In general, the value input to *T.Qual* uses $1/(1+|T.Qual|)$ to calculate the grid unit value; however, for $T.Qual > 100$, the grid unit value is $1/(1+|T.Qual-100|)$ and the program will reduce this value dynamically in regions where this would improve accuracy.

Chapter 3

ANALYSIS

The programs Poisson Superfish (PSF) and SIMION 8.1 were used to explore methods of focusing and phase shifting for the Houghton cyclotron. The cyclotron electromagnet, a GMW 3473-70 electromagnet, was modeled in PSF and then modified to calculate the magnetic field for various magnet adaptations. Each method attempted to produce a magnetic field that improved weak magnetic focusing. The model code is a modified version of the code for the Rutgers' cyclotron (see Appendix A).

To calculate ion trajectories, the magnetic field outputs from PSF were utilized with potential arrays made in SIMION in the shape of cyclotron Dees. These Dees were not the exact dimensions of the Houghton cyclotron as they were designed to model the Rutgers cyclotron. The only general variable in SIMION adjusted from the default settings was *T.Qual* which was set to 105 for all calculations. Variables created in the ion bench for this particular potential array were the amplitude of the radio-frequency voltage, rfV , which is in units of Volts and the resonance frequency which is expressed as an angular velocity, ω_0 (called 'omega' in the SIMION ion workbench), which is in units of rad/ μ s. The value $rfV = -1500$ V was used for all calculations, corresponding to a peak-to-peak voltage of 3000 V. The resonance frequency must be calculated using Eq. 36 for the specific magnetic field being applied. Throughout this chapter values of f_0 are given for the described magnetic fields. However, while ω_0 is equal to $2\pi f_0$, it is not recommended to calculate ω_0 from these values because the variable in SIMION is sensitive to many significant figures and should be calculated to a better degree of accuracy for use in SIMION. The use of approximate values for ω_0 will cause phase shifting.

While the coordinate system used for Section 2.1 is intuitive for cyclotron geometry, these models have different coordinate systems that must be noted. The PSF model uses two-dimensional Cartesian coordinates, and so it has x- and y-axes. This means for these calculations, the axial direction is the y-

direction, and the radial direction is the x-direction. The ion workbench in SIMION created for the Rutgers cyclotron and used in this project has a different coordinate system so for calculations from SIMION, the axial direction is the x-direction and the y- and z-axes are radial as shown in Figure 6. Whenever possible, the directions are simply referred to as axial or radial in order to minimize confusion.

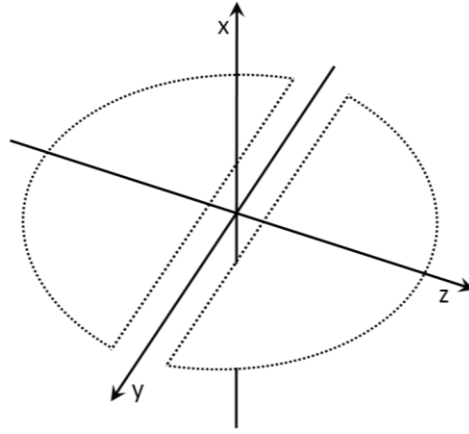


Figure 6: Dee configuration in SIMION. The y-z plane intersects at $x=25.5$ mm.

3.1 Unmodified

In order to evaluate the shape of the magnetic field produced by the unmodified Houghton cyclotron magnet, a two-dimensional model of the cyclotron magnet was made using PSF in the dimensions shown in Figure 7. For the most part the geometry is standard – two steel poles, a steel yoke, electromagnet coils, and an air gap where the chamber sits – however, the top pole also has a narrow air gap through its center. This gap exists to facilitate a mechanism that makes the pole position adjustable.

The PSF model assumes an infinite z-axis in its Cartesian calculations, so this configuration technically does not have electromagnet coils, rather it has infinitely long wires with set current densities on either side of each pole, the current of each moving in opposite directions.

This method of modelling requires a known current density value for the Houghton electromagnet; however, the current density of our cyclotron magnet was not listed in the magnet manual and the units used by PSF for current density were unknown. Instead, the value used for current density in the PSF model was determined by creating a plot of current density (in PSF units) versus the maximum magnetic field strength for this geometry as calculated by PSF using that value of current density. This plot is seen in Figure 8. The resulting linear trend was used to find a current density value of 22821 PSF units which corresponds to the magnetic field strength of 1.268 T, the manufacturer's measured value of the magnetic field strength for this geometry (39 mm pole gap, 150 mm pole face) with a coil current of 70 A.

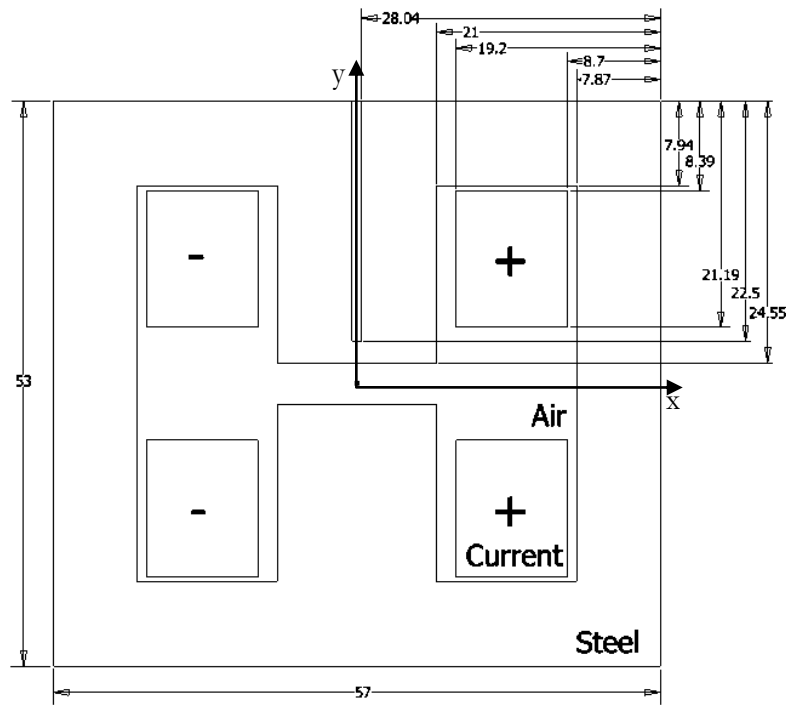


Figure 7: Schematic of the 2D representation of the unmodified cyclotron magnet. The PSF model used for the unmodified cyclotron magnet. All dimensions are in millimeters. The +/- current refer to into/out of the page.

The most thorough measurements conducted by the magnet manufacturer for the Houghton cyclotron magnet used a pole gap of 50 mm. Therefore, in order to compare the PSF calculation to this measurement of the magnetic field, the pole gap in the PSF geometry was increased to 50 mm. A linear trend for this geometry relating current density to maximum magnetic field strength was found in the same way as described above for the 39 mm pole gap. The equation of the line was found to be $J = 22501B$ where J is current density in PSF units and B is magnetic field strength in Teslas. As the manufacturer measured a maximum magnetic field value of 0.68868 T, the current density used for this PSF calculation was 15496 PSF units. The comparison of this calculated magnetic field with the manufacturer's measured values is shown in Figure 9. This comparison shows reasonable agreement, so the PSF model was assumed to be reasonably accurate for the 39 mm pole gap as well.

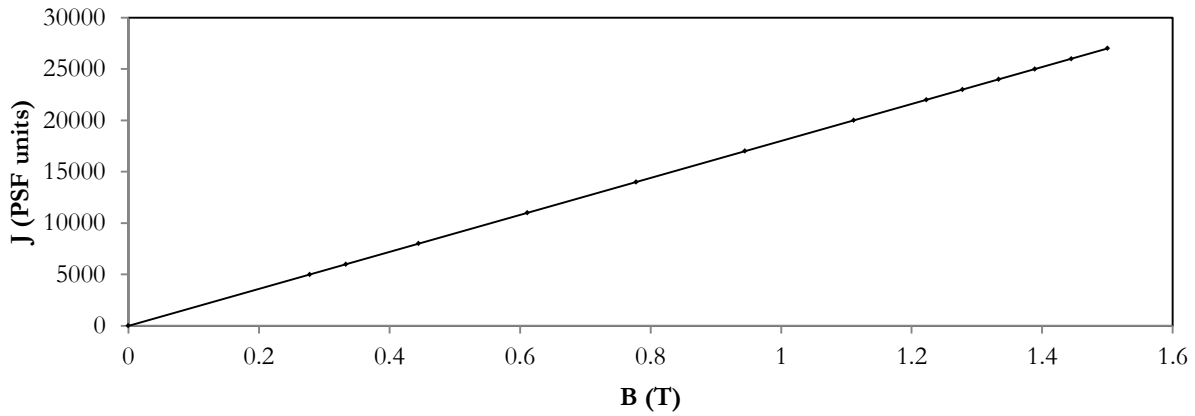


Figure 8: A calibration for current density for PSF shown using current density vs. maximum magnitude of the magnetic field as calculated by PSF. The line goes through 14 data points as calculated by PSF taken from current density values ranging from 0-27000. The equation of the line is $y=17998x$.

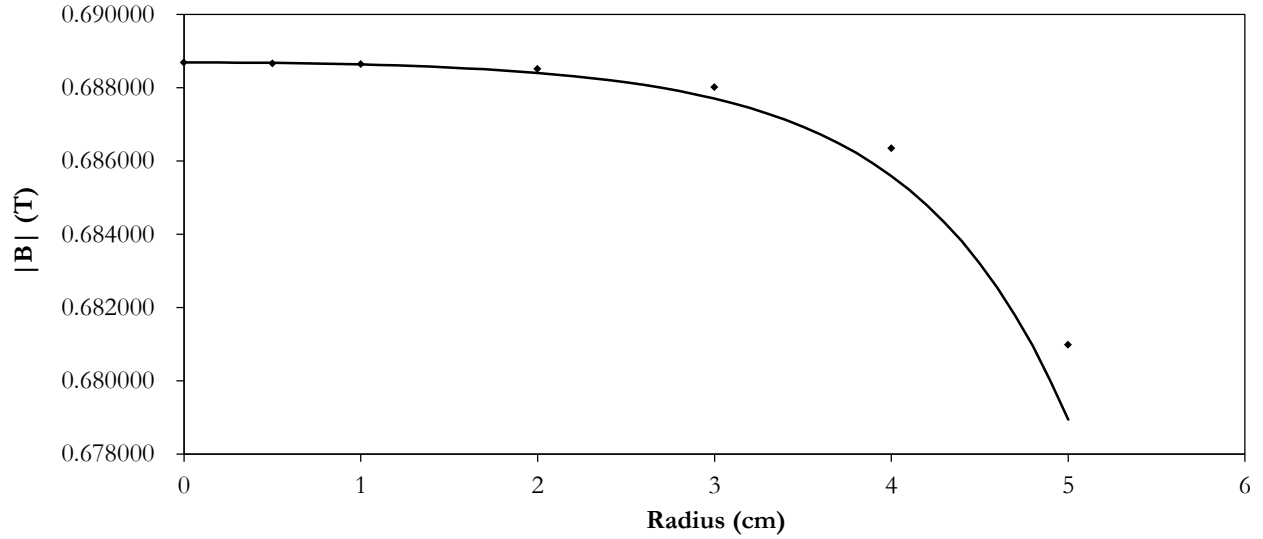


Figure 9: An analysis the reliability of PSF calculations shown using magnetic field vs. radius of PSF calculations (line) and manufacturer measurements (points). With the exception of $r=0$, the manufacturer's data points are averages of two measurements taken at the same radius from the center.

Returning to the Houghton magnet geometry, the magnetic field was calculated in PSF. Figure 10 shows the magnetic field lines and field contours from the PSF calculation. The magnetic field shape is as expected. The field contours are fairly parallel between the poles with fringing seen near the edges of the poles. The field contours are densest and the vector arrows are largest inside the magnet poles and yoke indicating the strongest field strength in these regions. Inside the pole gap, the strength of the magnetic field decreases as the radius from the center increase. The magnetic field is much weaker in the air regions compared to the steel regions (except for in the pole gap.)

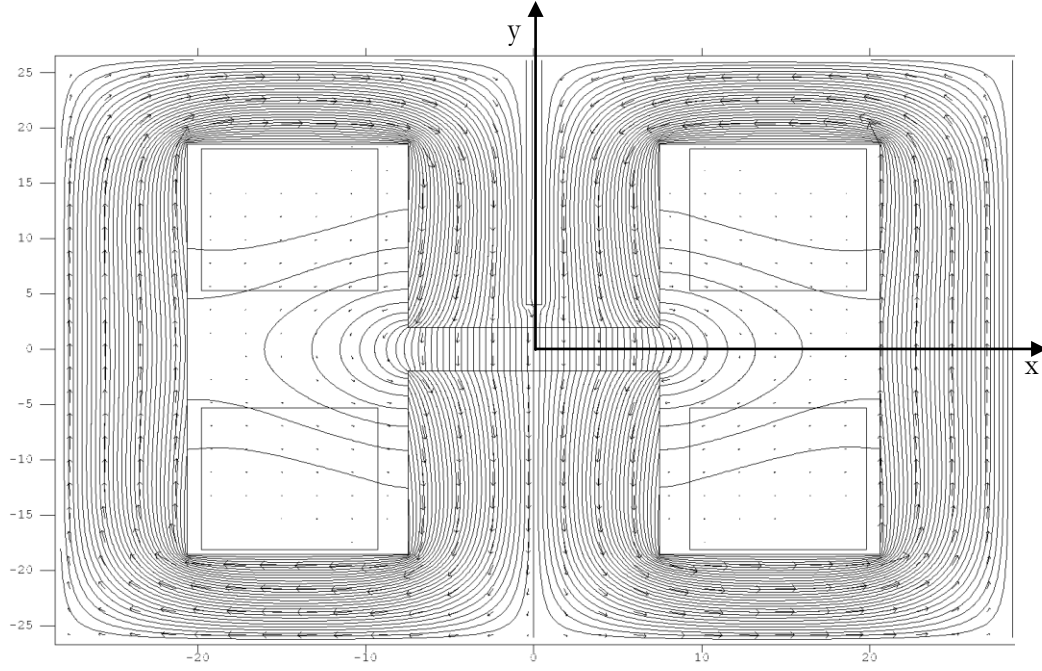


Figure 10: PSF calculation of the magnetic field of the unmodified magnet as field contours with vector arrows. Axes are in centimeters.

Figure 11 shows a plot of the magnetic field in the central plane between the magnet poles. The magnetic field appears fairly linear until around $r = 4.5$ cm at which point the magnetic field strength begins to decrease with increasing rapidity. The maximum magnetic field strength is 1.27 T, and according to Eq. 36 and Eq. 37, this corresponds to a Dee frequency of $f_0 = 19.3$ MHz and a maximum kinetic energy of 0.47 MeV for protons. Furthermore, Eq. 6 was applied to the PSF calculation of the magnetic field to produce a plot of the field index as it changes with radius as seen in

Figure 12. As PSF does not actually output $\frac{dB_y}{dx}$, the rate of change of the axial component of the

magnetic field with respect to radius, this value was approximated by finding $\frac{B_{y2} - B_{y1}}{\Delta x}$ for successive

values of x where $\Delta x = x_2 - x_1$ is the x step size chosen for the PSF calculation output. The field index, n was then evaluated at each point, and $n = 0.2$ occurred at 5.9 cm.

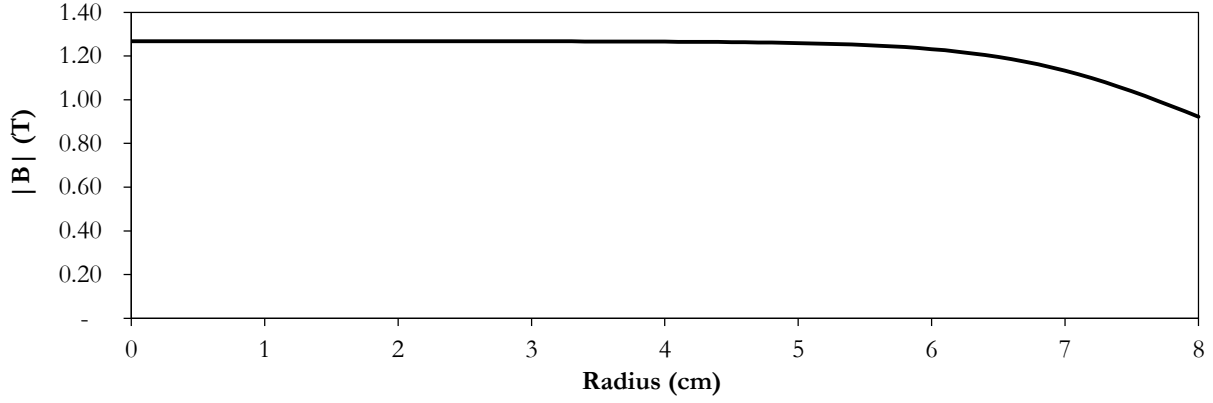


Figure 11: Magnetic field vs. radius in the central plane for the unmodified magnetic field according to PSF calculation.

Figure 11 shows a plot of the magnetic field in the central plane between the magnet poles. The magnetic field appears fairly linear until around $r = 4.5$ cm at which point the magnetic field strength begins to decrease with increasing rapidity. The maximum magnetic field strength is 1.27 T, and according to Eq. 36 and Eq. 37, this corresponds to a Dee frequency of $f_0 = 19.3$ MHz and a maximum kinetic energy of 0.47 MeV for protons. Furthermore, Eq. 6 was applied to the PSF calculation of the magnetic field to produce a plot of the field index as it changes with radius as seen in

Figure 12. As PSF does not actually output $\frac{dB_y}{dx}$, the rate of change of the axial component of the

magnetic field with respect to radius, this value was approximated by finding $\frac{B_{y2} - B_{y1}}{\Delta x}$ for successive

values of x where $\Delta x = x_2 - x_1$ is the x step size chosen for the PSF calculation output. The field index, n was then evaluated at each point, and $n = 0.2$ occurred at 5.9 cm.

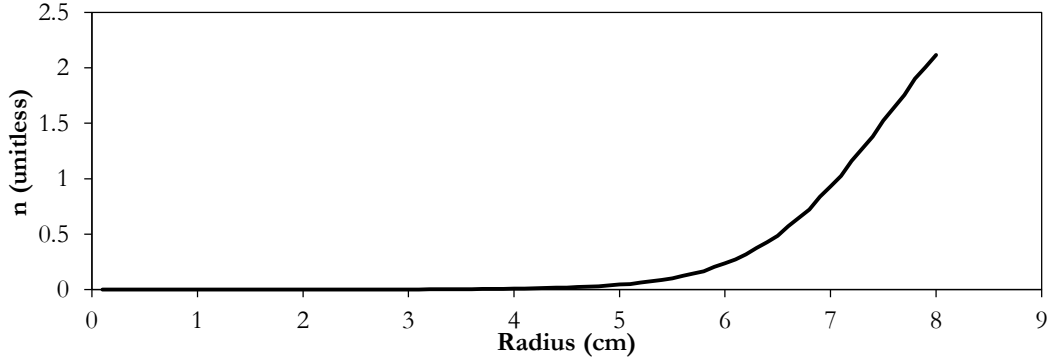


Figure 12: Field index vs. radius in the central plane for the unmodified magnetic field according to PSF calculation. The value $n=0.2$ occurs at $r=5.9$ cm.

The PSF calculation of the magnetic field was exported to SIMION, and the trajectory of a proton which started between the Dee electrodes was calculated as shown in Figure 13. As predicted by Eq. 37, the amount by which the radius increases for each successive rotation decreases as radius increases. The maximum radius reached is 51.5 mm, 27.5 mm short of the Dee radius. The proton does not go past this radius because after this point it begins to spiral back in towards the center. This occurs because the ion is out of phase, a process described in Section 2.1.4. While Figure 13 may falsely suggest a planar trajectory, Figure 14 shows the ion oscillations in the axial direction. The ion starts in the central plane, at $X=25.5$ mm, with no kinetic energy and oscillates around the central y - z plane. The amplitude of oscillations decreases as a result of magnetic focusing at larger radii. Notably the ion appears to come to equilibrium 0.5 mm below the center line, possibly as a result of the asymmetry caused by the air gap seen in Figure 7 through the top magnet pole.

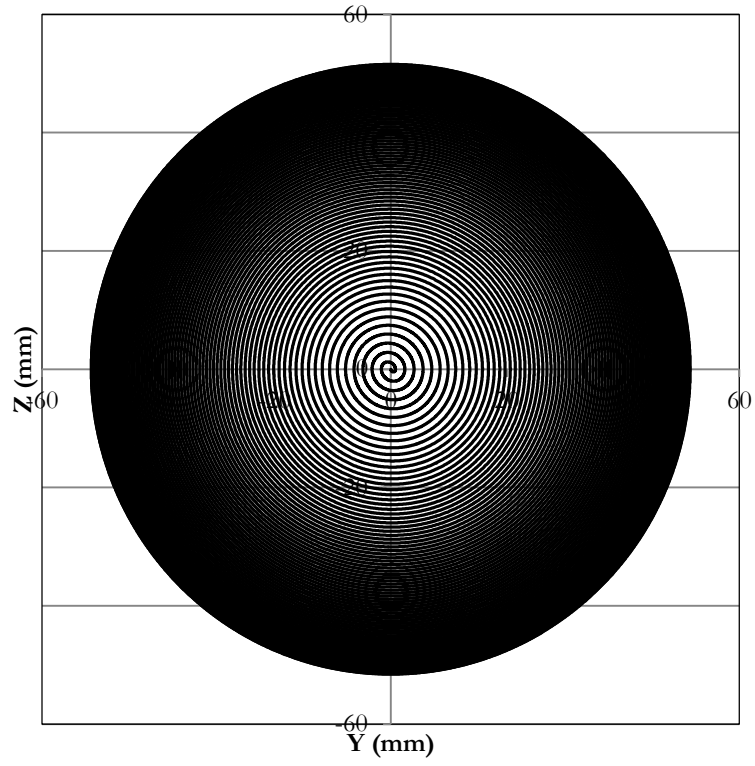


Figure 13: Proton trajectory in the unmodified cyclotron magnetic field as calculated by SIMION. $rfV=-1500$ V, $\omega=121.491$ rad/ μ s.

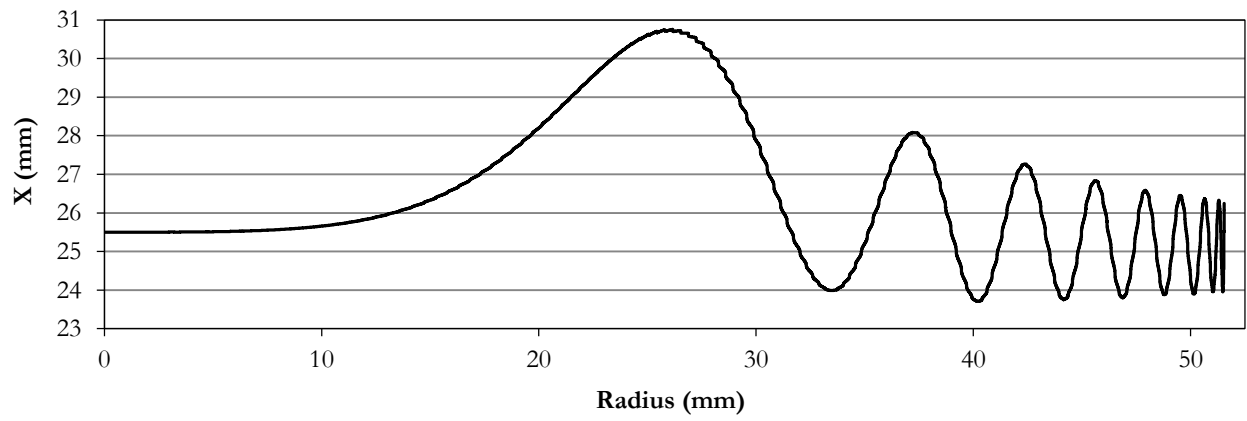


Figure 14: SIMION calculation of the axial position versus radius for the unmodified cyclotron magnet. $rfV=-1500$ V, $\omega=121.491$ rad/ μ s.

In order to test the degree to which SIMION calculations agreed with an analytical solution for the field input, the frequency of axial oscillations as described by Eq. 33 was calculated for the PSF magnetic field output, and this calculation was compared to a rough analysis of this value for SIMION's calculated ion trajectory as seen in Figure 15. The analytical solution used Eq. 33 and the values of n and f_0 calculated for the magnetic field as has been described. This particular analysis was done using $rfV = -3000$ V, so the exact values are not comparable to the analysis above.

An approximation of the axial frequency of oscillations for an ion trajectory calculated in SIMION was done using an averaging method. Each time the ion path crossed $X=25.5$ mm (which corresponds to the central plane in SIMION) with an upward velocity, the time of flight was noted. The time difference between successive points was considered to be the period of one oscillation. A frequency was calculated as the inverse of this period, and considered to be the axial frequency at the larger radius at which the time of flight had been recorded. It was found that for smaller radii where the axial oscillations are still large, a better approximation could be made by using this process but breaking the wave into halves or quarters, where the wave maximum was considered the first quarter, the point where the ion crosses $X= 25.5$ mm with a downward velocity was considered the half mark, the wave minimum was considered the three-quarter mark, and the end of the wave was the same as described above. The SIMION data points plotted in Figure 15 splits the first wave into quarters (such that it is consists of the first four data points) and the second wave in half.

When considering weak magnetic focusing, the magnetic field shape shown in Figure 11 is problematic. As discussed in Section 2.1.3, a linear decrease in magnetic field strength will improve weak focusing. The methods of manipulating the magnet geometry described in the following sections try to achieve this desired magnetic field shape.

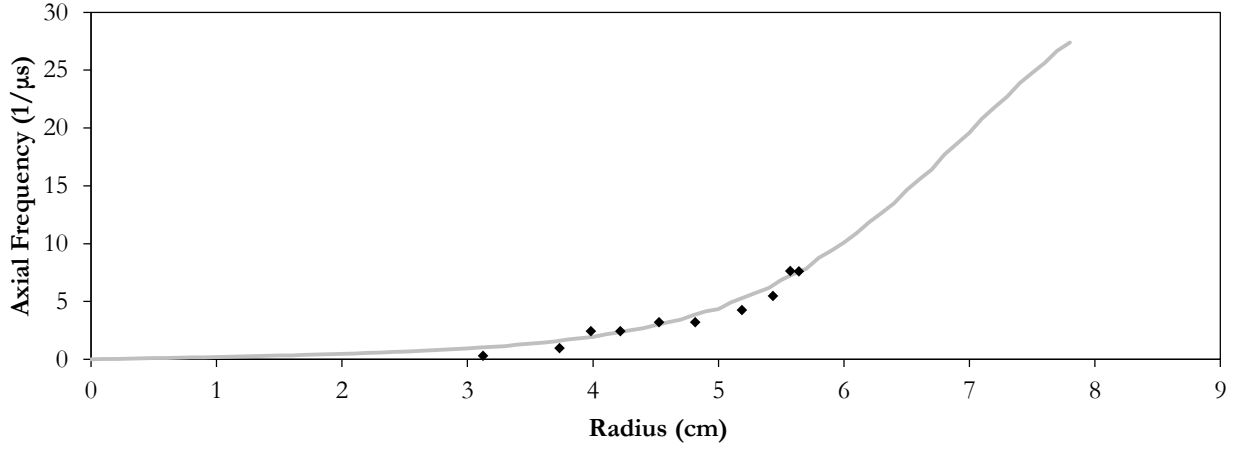


Figure 15: An analysis of the frequency of axial oscillations about the central plane versus radius. This compares the value calculated for the magnetic field that was used as in input for SIMION (grey line) to the frequency of oscillations recorded in the SIMION calculated ion trajectory (black points). $rfV = -3000$ V, $\omega = 121.488$ rad/ μ s.

3.2 Shims

As shown by Eq. 12, a magnetic field in which B_z changes linearly with radius must also have a B_r that is constant with radius for a give axial position and which increases in strength with distance from the central plane. As such, the success of weak focusing modifications was evaluated by the linearity of the axial magnetic field as it decreased with r .

The magnetic field shape produced by the unmodified Houghton magnet as shown in Figure 11 can be made more linear by increasing the strength of the magnetic field more near the center of the chamber than near the edge. The method of shimming was used to attempt this. Shimming involves placing thin iron sheets between the magnet pole and the vacuum chamber. This effectively slightly increases the gap outside of the shim which slightly decreases the magnetic field strength outside the shim. Shimming directs more of the field lines through the shim which slightly increases the magnetic field strength where there is a shim.

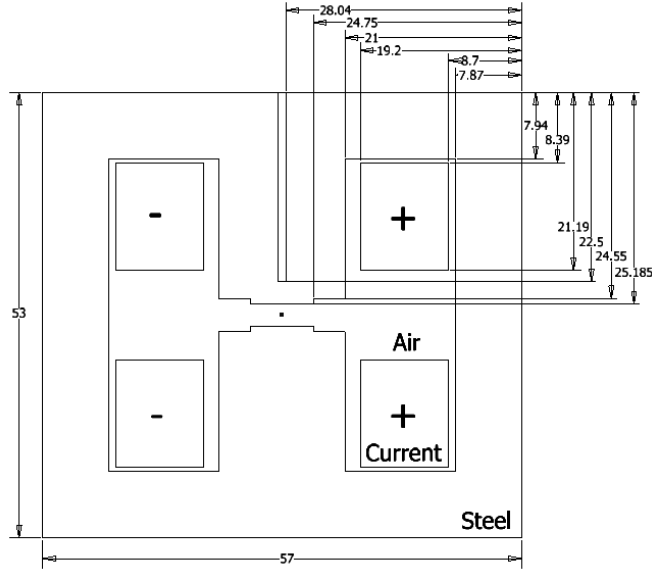


Figure 16: Schematic of the 2D representation of the shimmed cyclotron magnet. The PSF model used for the unmodified cyclotron magnet. All dimensions are in millimeters. The +/- current refer to into/out of the page.

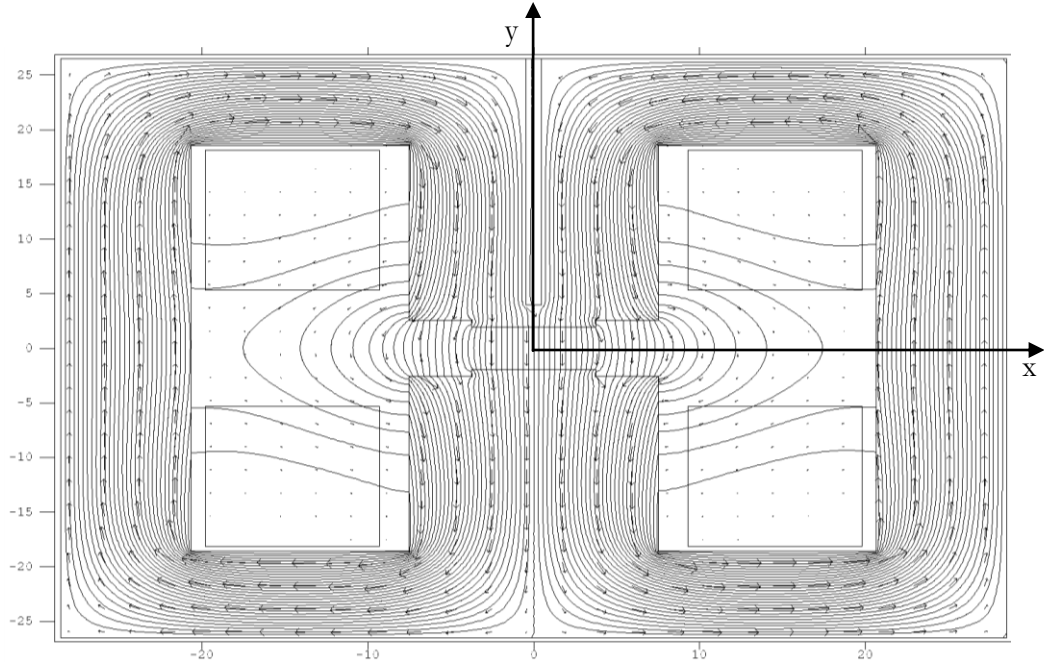


Figure 17: PSF calculation of the magnetic field of the shimmed magnet as field contours with vector arrows. Axes are in centimeters.

As one of the first techniques used historically for shaping the magnetic field in cyclotrons, shimming has been attempted with iron sheets of a variety of shapes, sizes, and configurations. For the Houghton cyclotron, circular magnetic steel shims with 0.3175 cm, 0.635 cm, and 1.27 cm thicknesses were modeled in various configurations. The magnetic field shape as calculated by PSF, vertical oscillations as calculated by SIMION, and the corresponding field index were compared to the values desired for focused orbit stability.

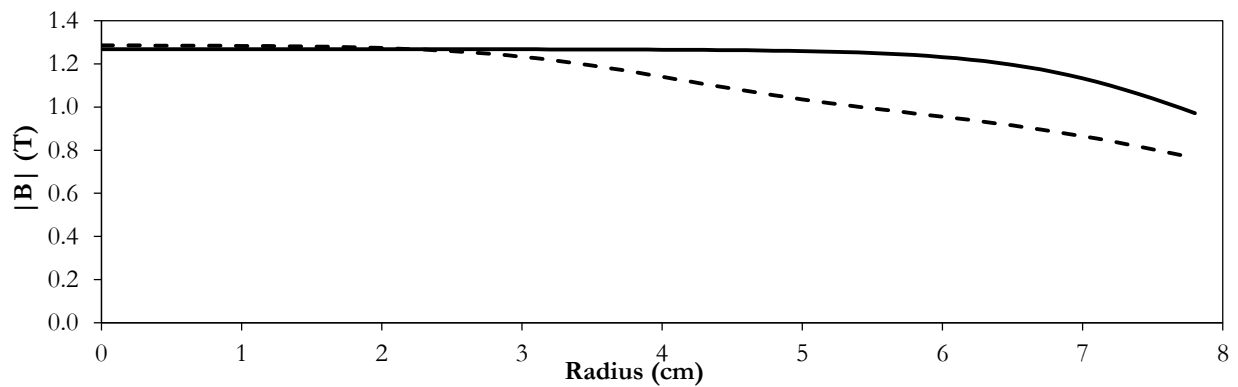


Figure 18: A comparison of the magnitude of the magnetic field vs. radius for the unmodified magnet geometry (solid line) and the single shim geometry (dashed line) according to PSF calculations.

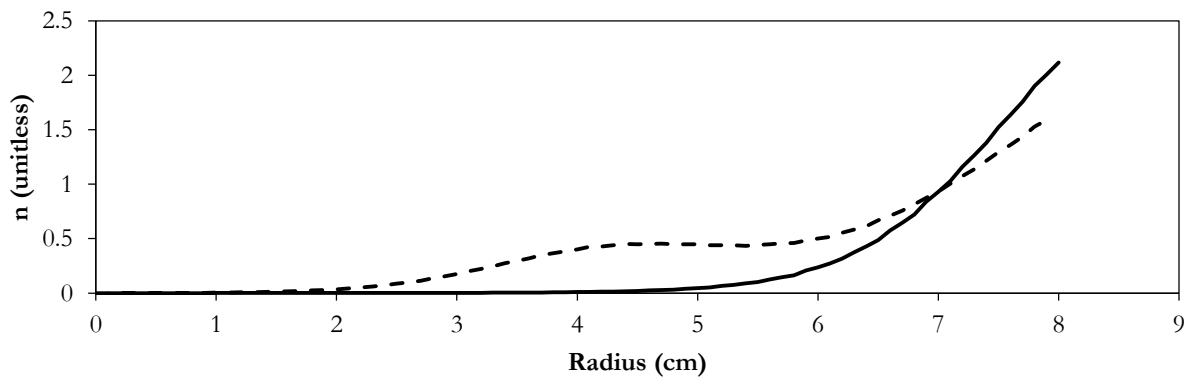


Figure 19: A comparison of field index vs. radius for the unmodified magnet geometry (solid line) and the single shim geometry (dashed line) for PSF calculations. $n=0.2$ occurred at $r=5.9$ cm for the unmodified and at $r=3.2$ cm for the lid.

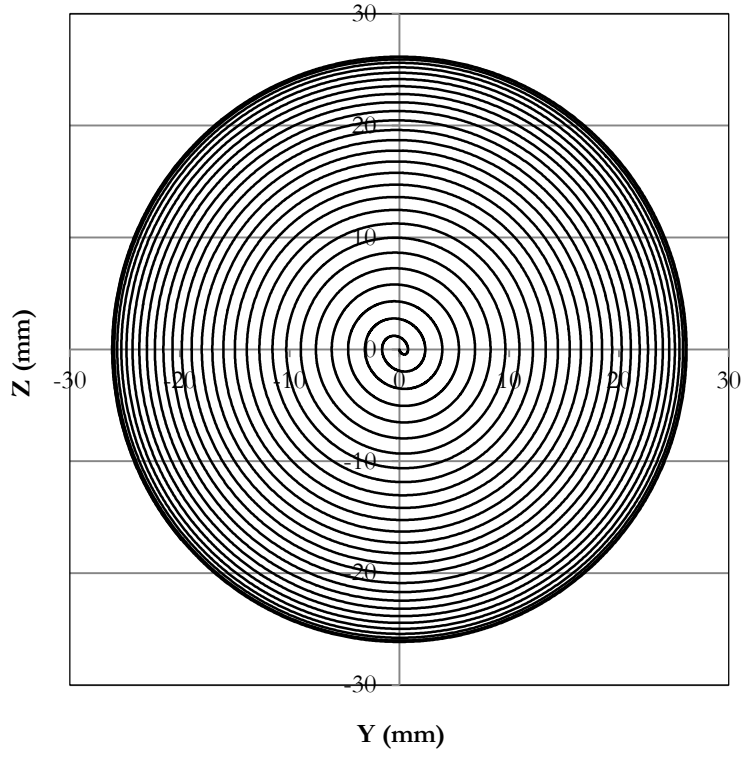


Figure 20: Proton trajectory in the SIMION calculation for the shimmed magnetic field. $rfV = -1500$ V, $\omega = 123.116$ rad/ μ s.

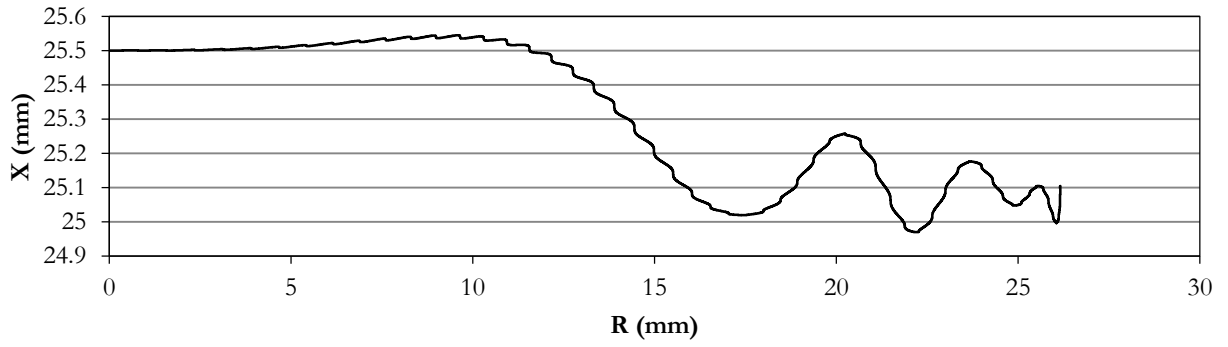


Figure 21: Axial position versus radius in the shimmed field according to SIMION calculations. The central plane is at $X = 25.5$ mm. $rfV = -1500$ V, $\omega = 123.116$ rad/ μ s.

Using the shim configuration described in Section 3.2, the ion path in SIMION is given in Figure 20. The maximum radius reached is 30.0 mm. As alluded to in Section 3.2, the ion does not reach a large radius because the magnetic field changes too quickly near the edge of the shim. This is a result of making the shim too thick.

Figure 21 shows the ion oscillations in the axial direction. The ion starts at the center, $X = 25.5$ mm. Figure 22 repeats the analysis of the axial oscillations described in Section 3.1 but with the magnetic field modified by the insertion of shims. The first two waves were split in half and plotted as two data points each.

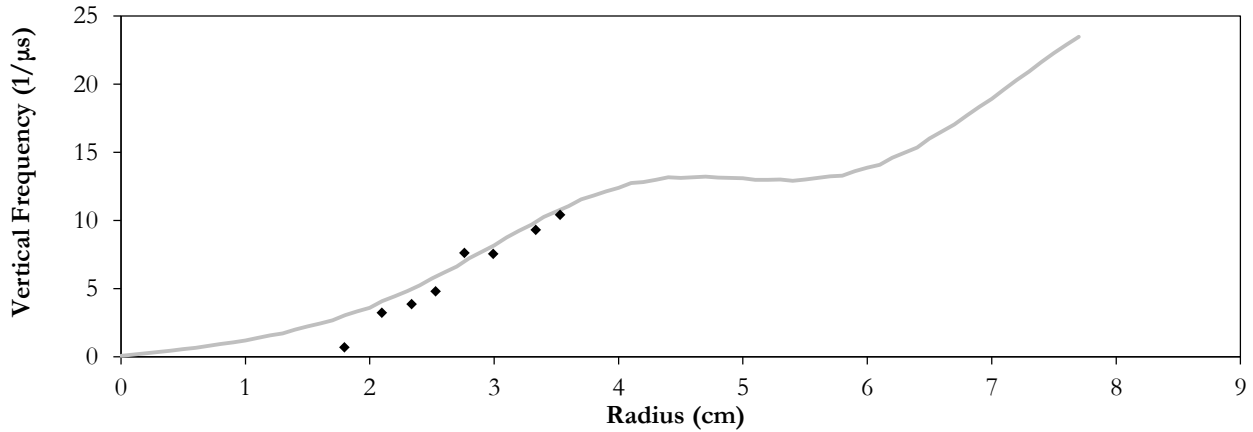


Figure 22: Frequency of axial oscillations about the central plane versus radius for the shimmed magnetic field. This compares the value calculated for the magnetic field that was used as input for SIMION (grey line) to the frequency of oscillations recorded in the calculated ion trajectory (black points). $rfV = -3000$ V, $\omega = 121.488$ rad/μs.

Given the historical success of shimming methods, it is likely that the failure of the shimmed design presented here is more associated to a failure to find the correct shimming configuration than it is a failure of the method itself. The shim plate thickness of 0.635 cm was used as an attempt to mimic the success of Lawrence's shimming design; however, it would have been wise to take into account the much smaller size of the Houghton cyclotron. In retrospect it appears that these shims were far too thick and created too dramatic of a change in magnetic field. While shims could still be used with the

Houghton cyclotron, the thin shims these calculations suggest would be challenging to make and keep positioned on the cyclotron so other focusing methods were explored.

3.3 Trim Coils

Trim coils placed strategically around the magnet poles can also affect the shape of the cyclotron magnetic field. As with the shimming method, the goal was to improve weak magnetic focusing by increasing the linearity of the magnetic field with radius. While initially the trim coil method was attempted in such a way that mimicked the field alteration desired by shimming (but which could be more easily tuned by changing the current in the coils or the number of coils used), many of the problems that occurred with shimming were reproduced here such that an alternate method of using the trim coils to buck the field was also attempted.

This method uses concentric trim coils as shown in Figure 23. A set is positioned between the chamber and each pole face as shown in Figure 24. The trim coils all have currents that are parallel to each other, so the magnetic field produced by the coils sums to the greatest magnitude at the center. An adding method for trim coils aligns the current direction in the coils with the current direction in the electromagnet as shown in Figure 25.

This increases the strength of the magnetic field the most at the center where the magnetic fields of all of the trim coils are superimposed. The magnetic field strength is slightly increased at mid-regions where the radius is still inside larger trim coils but is past inner trim coils because, by the right-hand rule, the inner trim coils would then be bucking the field in this region. Therefore, the magnetic field is increased more near the center relative to the increase that occurs at the edge. One issue with this method is that in order to avoid problems with phase shifting, B_z must stay as constant as possible; however, an adding method of trim coils creates a more linear magnetic field but with a steeper slope. This is in contrast to bucking which creates a more linear magnetic field but which decreases the slope steepness.

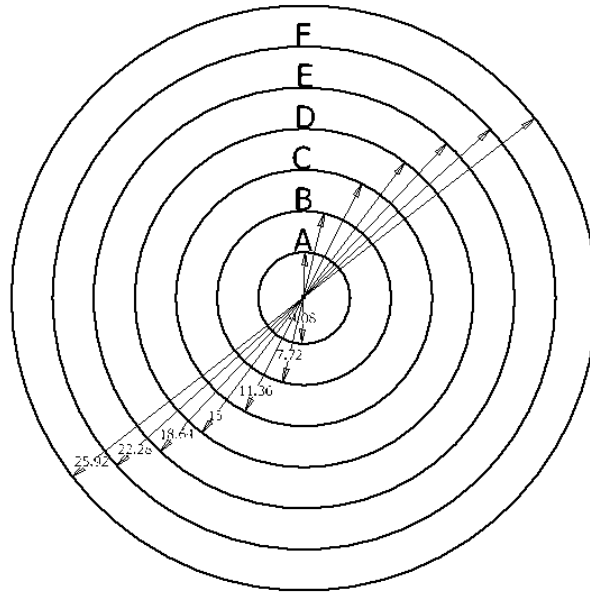


Figure 23: Trim coil geometry. The central circle is empty, and each capital letter denotes a particular trim coil. All diameters are in centimeters.

By configuring the current direction in the trim coils such that it is anti-parallel the current in the electromagnet, as shown in Figure 25, magnetic field bucking is essentially the reverse of the adding method. The magnitude of the combined magnetic fields of the trim coils is still greatest at the center where the magnetic fields of all of the trim coils are superimposed; however, this magnetic field is in the opposite direction to the magnetic field produced by the electromagnet coils. Therefore, the magnetic field strength is decreased the most at the center and slightly decreased at mid-regions where the radius is still inside larger trim coils but is past inner trim coils because, by the right-hand rule, the inner trim coils would then be adding to the field in this region. Therefore, the magnetic field is decreased more near the center relative to the decrease that occurs at the edge. As bucking reduces the maximum magnetic field strength which, according to Eq. 37, kinetic energy is dependent on the square of, trim coils must be optimized to buck as little as possible while still producing the desired field shape.

By configuring the current direction in the trim coils such that it is anti-parallel the current in the electromagnet, as shown in Figure 25, magnetic field bucking is essentially the reverse of the adding method.

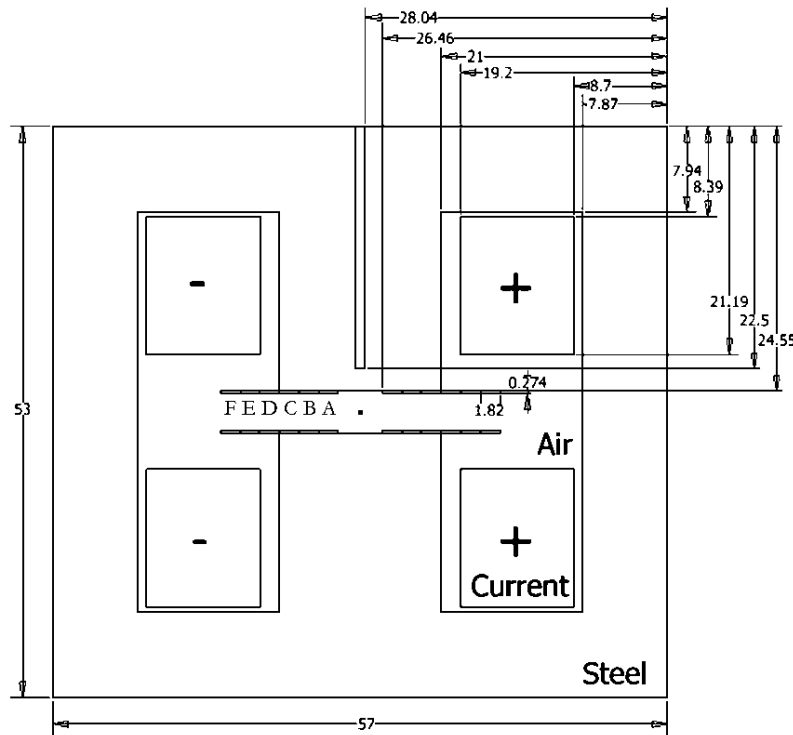


Figure 24: Schematic of the 2D representation of the cyclotron magnet with trim coils. Six focusing coil positions, A-F, were used on each side of each pole face. All dimensions are in millimeters. The +/- current refer to into/out of the page. For all calculations, one or more of the coils were unused and turned 'off,' setting the current density equal to zero.

The magnitude of the combined magnetic fields of the trim coils is still greatest at the center where the magnetic fields of all of the trim coils are superimposed; however, this magnetic field is in the opposite direction to the magnetic field produced by the electromagnet coils. Therefore, the magnetic field strength is decreased the most at the center and slightly decreased at mid-regions where the radius is still inside larger trim coils but is past inner trim coils because, by the right-hand rule, the inner trim

coils would then be adding to the field in this region. Therefore, the magnetic field is decreased more near the center relative to the decrease that occurs at the edge. As bucking reduces the maximum magnetic field strength which, according to Eq. 37, kinetic energy is dependent on the square of, trim coils must be optimized to buck as little as possible while still producing the desired field shape.

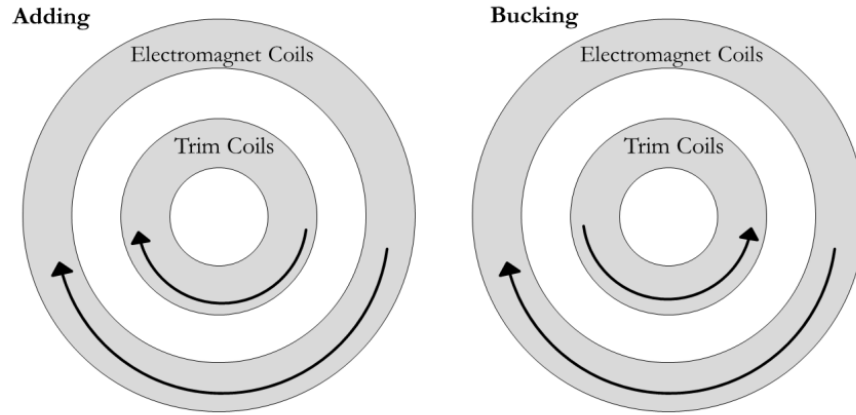


Figure 25: The current directions in adding and bucking trim coils. The arrows indicate the direction of the current in the coils. Current direction for adding field is parallel to the electromagnet coil; current direction for bucking field is anti-parallel to the electromagnet coil.

As seen in Figure 24, the trim coils were tested both between the pole face and the chamber and outside the pole radius. For both adding and bucking calculations various combinations of the trim coils were used and various current densities in the coils were attempted. The values of current density were chosen as an attempt to systematically alter the magnetic field to the desired shape.

For an adding field, Table 1 describes which coils were used for various calculations in PSF and the corresponding current densities. In order to facilitate easy comparison, the sum of the current densities for each calculation was kept at 1500 PSF units. This kept the maximum magnetic field strength fairly constant, as seen in Figure 26, which made it easier to evaluate the shape.

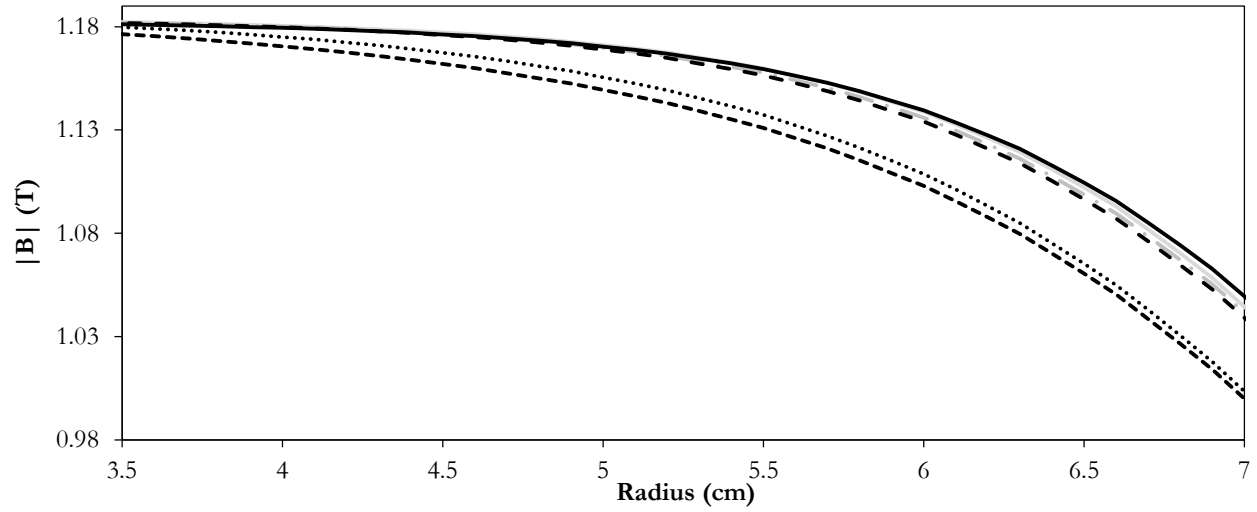


Figure 26: Magnetic field strength versus radius for various configurations of trim coils. Both axes have been truncated to make the variance easier to see – from $0 \text{ cm} < r < 3.5 \text{ cm}$, B stays basically constant for all plots around $B=1.18 \text{ T}$. The plots, listed going up the y-axis and using the calculation numbers in Table 1, are 1 (black small dashed), 2 (black dots), 5 (black dot-dashed), 4 (grey dashed), 3 (grey solid), 6 (black solid).

Figure 26 indicates that the adding method of trim coils is only effective up to a point. No attempted combination of trim coils with current densities that sum to 1500 extended $n = 0.2$ past $r = 5.8 \text{ cm}$, 2 cm short of maximum radius. This is actually worse than the unmodified magnetic field for which $n = 0.2$ occurred at $r = 5.9 \text{ cm}$.

This analysis was repeated with a bucking field. The same magnitudes were used for current density as seen in Table 1, but the polarity was switched such that it was anti-parallel to the electromagnet current. The magnetic field shape is seen in Figure 27.

Table 1: Reference table for trim coil comparison calculations and the corresponding radii at which $n=0.2$. For ‘adding’ current densities were polarized such that the direction of the current was set parallel to the electromagnet current for the corresponding side. For ‘bucking’ current densities were polarized such that the direction of the current was set anti-parallel to the electromagnet current for the corresponding side.

Calculation Number	Coils (Figure 24) used and corresponding current density (PSF units)	Adding: r (cm) where $n \geq 0.2$	Bucking: r (cm) where $n \geq 0.2$
1	A: 75, B: 475, C: 950	5.5	6.1
2	B: 350, C: 1150	5.5	6.1
3	D: 1500	5.8	5.9
4	C: 250, D: 450, E: 800	5.8	5.9
5	C: 400, E: 1100	5.8	5.9
6	F: 1500	5.8	5.8

Careful observation of Figure 27 reveals that for some configurations tried, the magnetic field actually increases in magnitude out to around $r = 5$ cm at which point it begins decreasing again. This is problematic because it yields a negative field index, as seen in Figure 28.

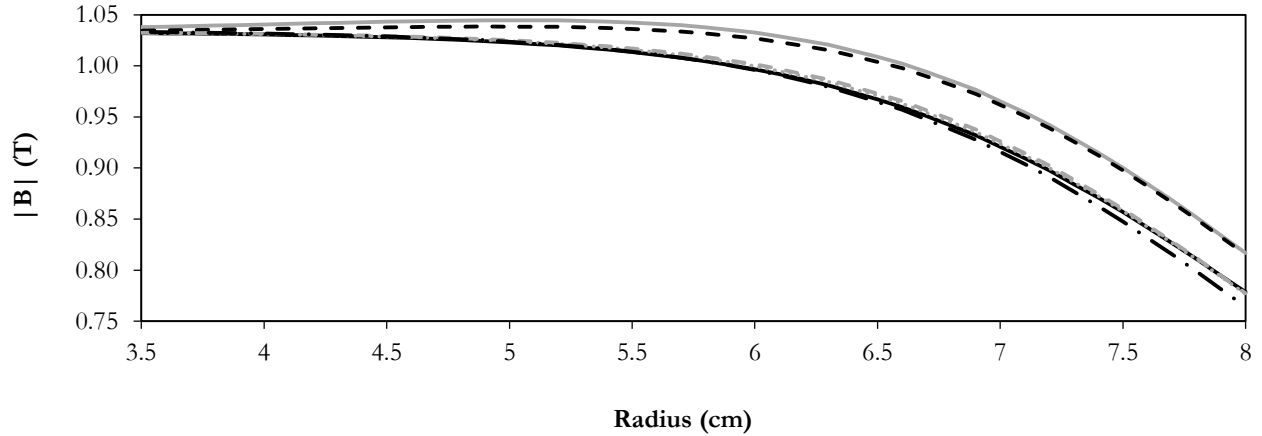


Figure 27: Magnetic field strength versus radius for various configurations of trim coils. Both axes have been truncated to make the variance easier to see – from $0 \text{ cm} < r < 3.5 \text{ cm}$, B stays basically constant for all plots around $B=1.03 \text{ T}$. The plots, listed going up the y-axis and using the calculation numbers in Table 1, are 6 (black dot-dashed), 3 (black solid), 4 (grey dot), 5 (grey dashed), 2 (black dashed), and 1 (grey solid).

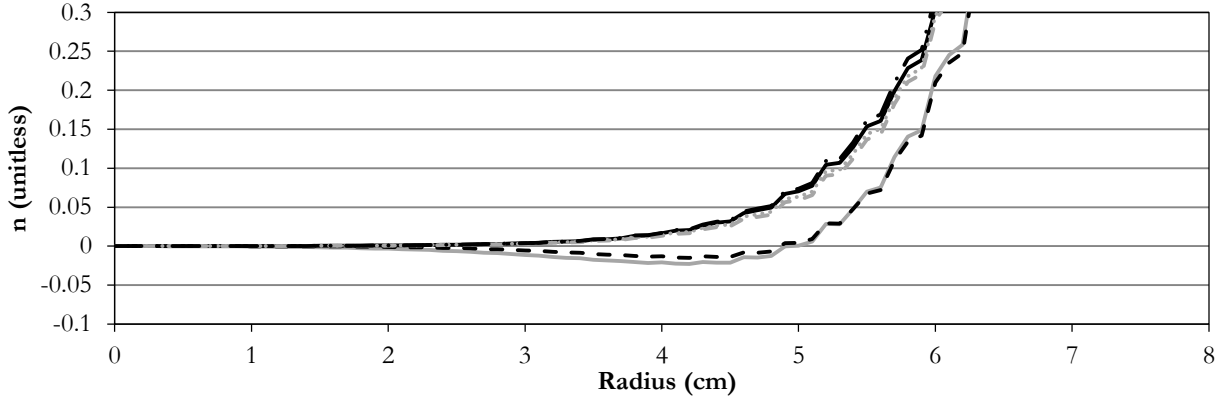


Figure 28: Field index versus radius for various configurations of trim coils. Both axes have been truncated to make the variance easier to see. The plots, listed going up the y-axis and using the calculation numbers in Table 1, are 6 (black dot-dashed), 3 (black solid), 4 (grey dot), 5 (grey dashed), 2 (black dashed), and 1 (grey solid).

The bucking method is minimally successful in configurations 1 and 3 in that it moves $n = 0.2$ out to further radii and does not yield negative values for n ; however, the difference in radius is minimal – about 0.2 cm – and comes at the steep cost of a $\sim 20\%$ reduction in maximum magnetic field from 1.27 T to 1.07 T. As such, this modification was considered insufficient.

3.4 Chamber Lids

This method of altering the field, the most successful to date, involves replacing the vacuum chamber's aluminum lids with magnetic steel lids. As the vacuum chamber radius is 2.2 cm larger than the radius of the magnet poles, these lids act as wide pole faces that draw the magnetic field lines out to larger radii. This significantly increases the uniformity of the magnetic field in the region the cyclotron Dees occupy, as seen in Figure 29.

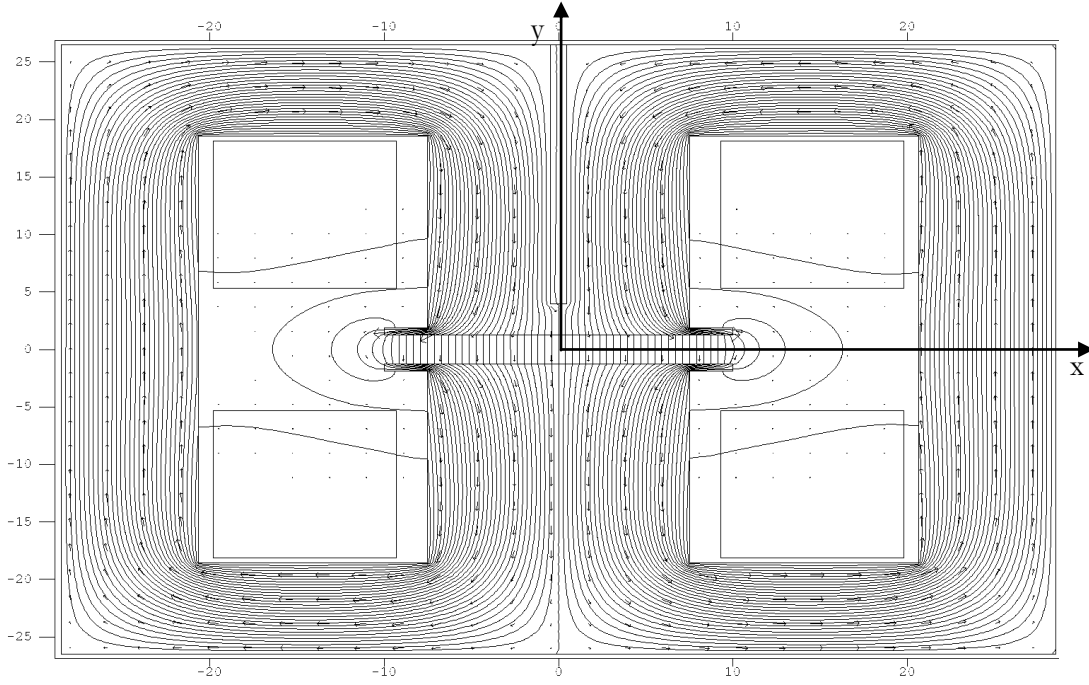


Figure 29: PSF calculation of the magnetic field of the magnet with steel chamber lids (10 cm radius) as field contours with vector arrows. Axes are in centimeters.

The most desirable magnetic field will change linearly with radius. Figure 30 shows the lids improve the linearity of the field. The maximum magnetic field of the unmodified design is $B = 1.27$ T and is $B = 1.77$ T for the lid design. This is because the pole gap of the unmodified design is 3.9 cm while the lid design has a pole gap of 2.54 cm. Using Eq. 36 and Eq. 37, $B = 1.77$ T corresponds to a Dee frequency of 27.0 MHz and a maximum kinetic energy of 0.91 MeV for protons.

The comparison of the field index versus radius for these magnetic fields as seen in Figure 31 essentially shows the rate of change of magnetic field versus radius. Notice that for the steel lid magnetic field, the $n = 0.2$ resonance occurs past the maximum Dee radius. While the linearity has clearly improved, there is still room for improvement.

The trajectory of a proton in this magnetic field as calculated by SIMION is shown in Figure 32. The maximum radius reached is 42.8 mm. While the maximum radius is small compared to the unmodified magnet (50.2 mm), the maximum magnetic field increases in this configuration, resulting in an overall increase in kinetic energy.

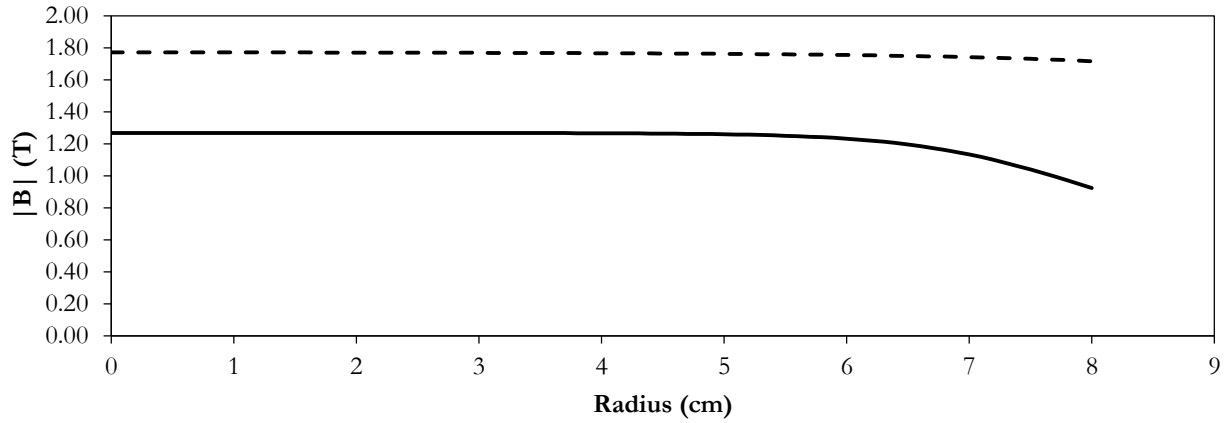


Figure 30: Magnitude of the magnetic field vs. radius for the unmodified cyclotron magnet (solid line) and for the steel lid design (dashed line). Current density of both calculations is 22860 PSF units. This is for Dee radius is 7.8 cm.

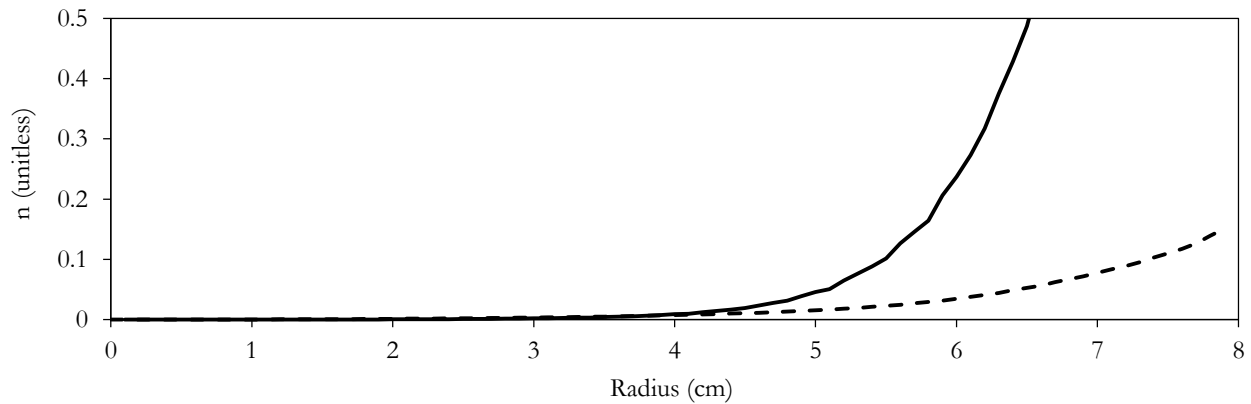


Figure 31: Comparison of the field index versus radius for the unmodified cyclotron geometry (solid line) and steel lid design (dashed line) from PSF calculations. $n=0.2$ occurred at $r=5.9$ cm for the unmodified and at $r=8.3$ cm for the lid.

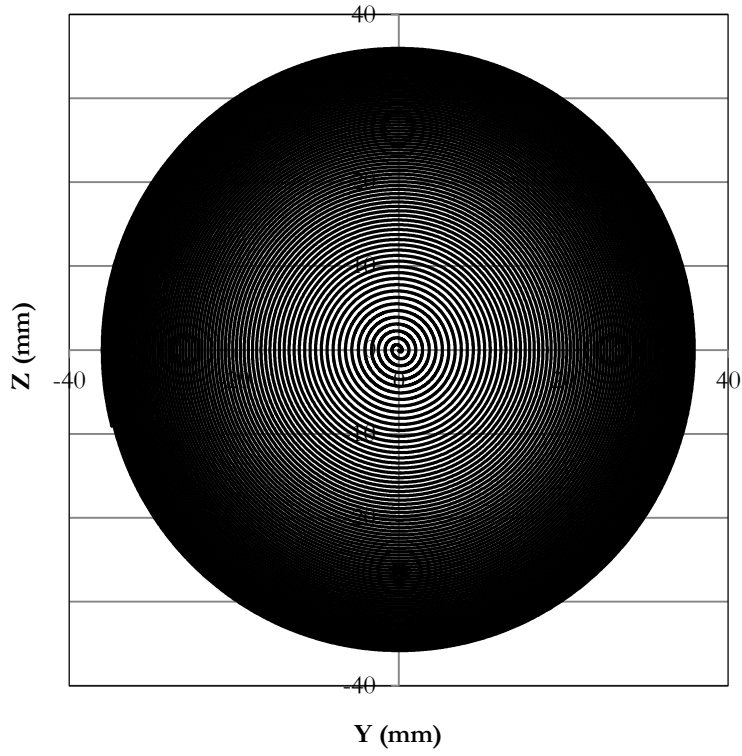


Figure 32: Proton trajectory in the SIMION calculation for the steel lid magnetic field. $rfV = -1500$ V, $\omega = 169.648$ rad/ μ s.

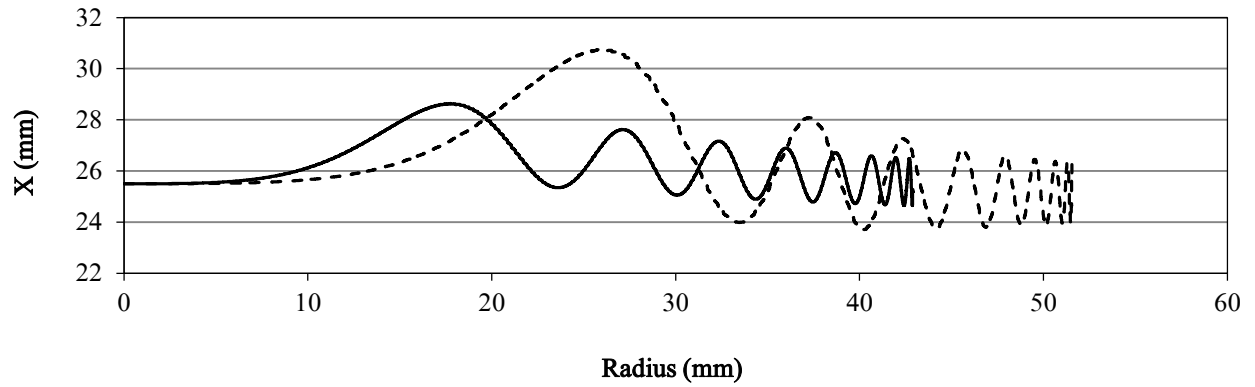


Figure 33: Comparison of the vertical oscillations versus radius for the steel lid magnetic field (solid) and unmodified magnetic field (dashed) according to SIMION calculations. The central plane is at $X = 25.5$ cm. $rfV = -1500$ V, $\omega = 169.648$ rad/ μ s.

Figure 14 makes abundantly clear the fact that the ion is actually experiencing a decent amount of focusing and, while better weak magnetic focusing will still be advantageous, collisions with the Dees is unlikely to be the major issue in the Houghton cyclotron. Rather, the phase shifting issue is far more pressing. Figure 35 considers the phase shift in terms of how the angle difference, $\Delta\theta = |\phi - \alpha|$, changes with radius where α is the azimuthal position of the ion as shown in Figure 34 and ϕ is an angular description of the phase of the oscillating Dee voltage. That is, considering Figure 34, if a proton is in the Dee gap at $\alpha = 0$ and the left Dee is at its minimum at $rfV = -1500$ V, then $\Delta\theta = 0$ because this is precisely the right time that the proton should be in the Dee gap in order to receive maximum acceleration. Therefore, this Dee voltage corresponds to $\phi = 0$. This angle can also be mathematically described as $\phi = \frac{\cos^{-1}(rfV)}{1500V}$. However, if the proton is in the Dee gap at $\alpha = 0$ and the left Dee is at $rfV = -1000$ V either because it is still dropping to the minimum value or it has passed $rfV = -1500$ V and started climbing again, $\alpha \neq \phi$ and $\Delta\theta$ is non-zero.

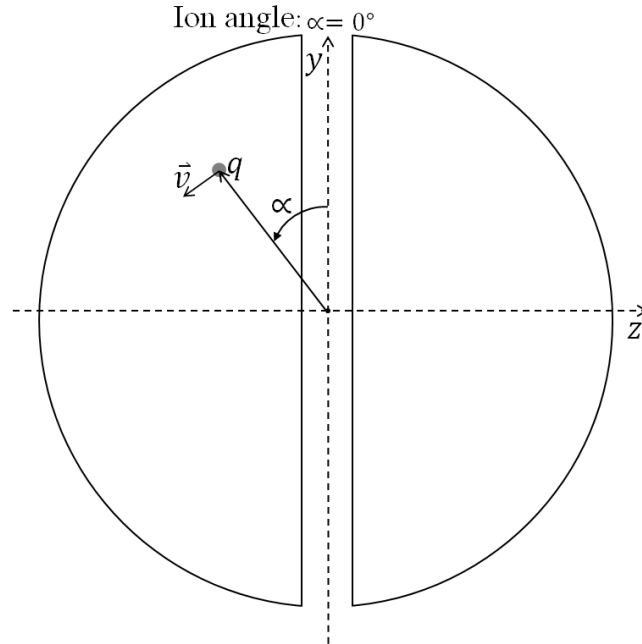


Figure 34: The azimuthal position of the ion in the chamber.

Figure 35 indicates that for the unmodified magnetic field, the phase shift will increase with radius until $\Delta\vartheta = \frac{\pi}{2}$ at which point the phase shift is too great and the ion starts losing energy. The value $\Delta\vartheta = \frac{\pi}{2}$ corresponds to the point at which when the ion reaches the center of the Dee gap, the potential difference equals zero. Considering Figure 35 again, beyond $\Delta\vartheta = \frac{\pi}{2}$, as the phase difference continues to increase, the left Dee will be at positive voltages such that the ion does not just receive less acceleration as it crosses the gap, but it actually begins to lose energy as it is repelled by the Dee that it is moving towards (and drawn to the Dee it is moving away from).

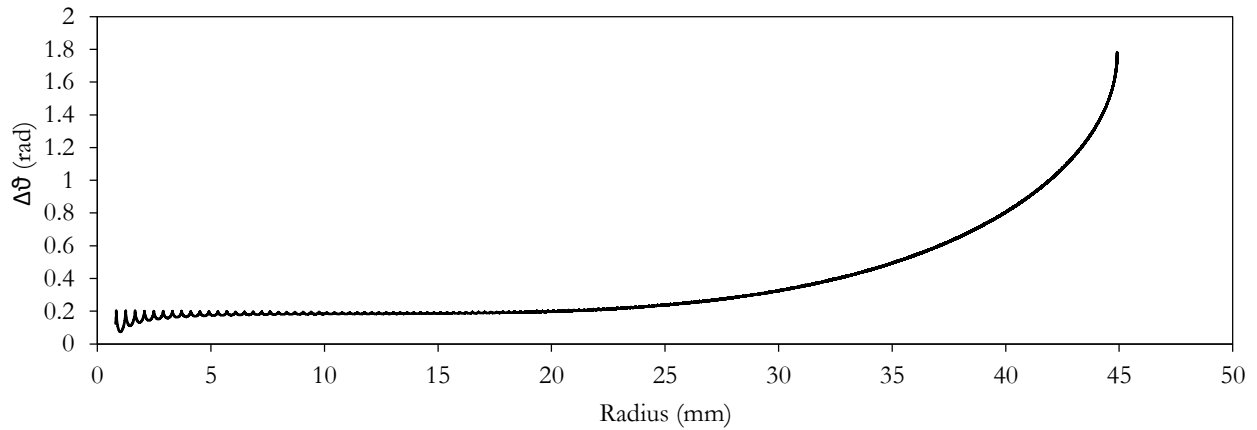


Figure 35: Angular phase difference versus radius for the steel lid magnetic field according to an analysis of the SIMION calculation. $rfV = -1500$ V, $\omega = 121.491$ rad/ μ s.

Chapter 4

CONCLUSION

4.1 Status and Future Plans

The methods described are design tools that can be used to understand and improve focusing in the Houghton cyclotron. Steel discs of the appropriate size have been purchased so that the PSF and SIMION calculations for the steel lid model can be tested by operating our cyclotron with these lids in place. Currently a new vacuum chamber is under construction for the cyclotron which has ports that will be welded to the chamber instead of glued with epoxy, an improvement expected to reduce leakage problems. In addition, the new design will use clamps instead of screws to hold the chamber lids down. This will eliminate the need to drill holes into the lid that line up exactly with the holes in the chamber. In addition, the clamp design will leave just enough room for the magnet poles to sit inside them, so the chamber will be easily positioned by simply fitting the pole into this space.

The magnetic field is being measured without the vacuum chamber in position so that a full scan of the central plane can be done; however, this will also require constructing a mount to hold the lids in place. In order to be used as actual lids on the cyclotron chamber, grooves for o-rings need to be machined into the plates and also a divot to accommodate the existing ion filament. PSF and SIMION calculations should be run with these modifications before it is added to the steel plates.

As has been discussed, while the steel lid offers several advantages, the phase shifting problem is too limiting to consider this a final solution. While PSF does not have the capabilities to model azimuthally varying pole tips, alternative modeling software should be considered to test this type of adaptation to the magnetic field. The software Maxwell 3D was used to model some azimuthally varied pole tips for the Rutgers cyclotron [26]. There are many possibilities for how this could be achieved including sectorized and spiraled pole tips. Depending on the type of azimuthal variation desired, this field may be achievable by milling sectors out of the steel lids.

Future projects could also modify these models of the cyclotron to be used in conjunction with the operating cyclotron. This would be a considerable task as it would require making a new potential array in Simion that uses the dimension of the Houghton cyclotron's Dees (as opposed to the Rutgers's Dees which have been utilized so far) and writing code that could be used in conjunction with PSF files and SIMION in order to calculate measureable variables for the cyclotron in such a way that would allow the cyclotron operator to assess the cyclotron's functionality.

Appendix A

POISSON SUPERFISH

This Appendix is an overview of how to use the software package Poisson Superfish (PSF) for the modelling and calculation methods described in this paper. PSF models two-dimensional static magnetic and electric fields. The PSF software package is made available as a free download from the Los Alamos National Laboratory website (http://laacg.lanl.gov/laacg/services/download_sf.phtml). This project uses the most current version, 7.19. This version is supported for Windows NT, Windows 2000, and Windows XP on Pentium or equivalent processors. The download is made available as a directory named “LANL” which must be copied into the C: drive. Section I of the manual file C:\LANL\Docs\SFINTRO.doc gives a detailed break-down of the memory requirements for Automesh and Poisson, the PSF programs used for this analysis.

The parameters for model calculations in PSF are described completely in user-generated geometry files. The geometry file specifies the type of problem being solved, the region limits for the problem, the mesh density to use for calculations, and coordinate points describing regions of various materials that

A.1 Geometry File

To create a geometry file (for Windows):

The simplest way to make a new geometry file is to begin with a complete geometry file for a similar problem and modify it. Below is the entire geometry file used for the unmodified electromagnet (with a few added comment lines to indicate which sections are being reference in the discussion that follows.) To use this text as a geometry file, copy it into a text editor and save it with the extension “.am” and follow the instructions below for calculating a geometry file.

Based on Rutgers 12-inch cyclotron magnet

```
;Pole face: 150mm, Pole gap: 39mm, Current: 70A
```

```
;NOTE: this is a slice down the middle of the magnet  
;where the pole piece is widest (this really should be a 3-D  
problem)
```

```
;  
;last modified September 28, 2013, 1719 hours
```

```
&reg kprob=0, ;poisson or pandira problem  
mode=-1 ;Used fixed gamma for material 2  
mat=2,  
nbslo=0, ;Dirichlet boundary condition on lower edge  
nbsup=0, ;Dirichlet boundary condition on upper edge  
nbslf=0, ;Dirichlet boundary condition on left edge  
nbsrt=0, ;Dirichlet boundary condition on right edge ;Dirichle
```

```
;----this section is for variable density mesh-----
```

```
XMINF=0,XMAXF=0,YMINF=-3,YMAXF=3,KMIN=120,KTOP=240,LMIN=0,LTOP=0;
```

```
XREG1=-20,XREG2=20  
kreg1=40,kreg2=181,kmax=221  
yreg1=-10,yreg2=10  
lreg1=40,lreg2=201,lmax=241 &
```

```
;-----
```

```
;begin Region 1  
&reg mat=2 &  
&po x=-28.50,y=-26.50 & ; Entire geometry is initially iron  
&po x= 28.50,y=-26.50 &  
&po x= 28.50,y= 26.50 &  
&po x=-28.50,y= 26.50 &  
&po x=-28.50,y=-26.50 &  
;end Region 1
```

```
&reg mat=1 & ; start of air region
```

```

&po x=-20.63,y= 18.56 &
&po x= -7.50,y= 18.56 &
&po x= -7.50,y=  1.95 &
&po x=  7.50,y=  1.95 &
&po x=  7.50,y= 18.56 &
&po x= 20.63,y= 18.56 &
&po x= 20.63,y=-18.56 &
&po x=  7.50,y=-18.56 &
&po x=  7.50,y= -1.95 &
&po x= -7.50,y= -1.95 &
&po x= -7.50,y=-18.56 &
&po x=-20.63,y=-18.56 &
&po x=-20.63,y= 18.56 &

```

```

&reg mat=1 & ; pole air region

```

```

&po x= -0.46,y= 26.50 &
&po x=  0.46,y= 26.50 &
&po x=  0.46,y=  4.00 &
&po x= -0.46,y=  4.00 &
&po x= -0.46,y= 26.50 &

```

```

&reg mat=1, cur=-22860& ; start of left-side top coil

```

```

&po x=-19.80,y= 18.11 &
&po x= -9.30,y= 18.11 &
&po x= -9.30,y=  5.31 &
&po x=-19.80,y=  5.31 &
&po x=-19.80,y= 18.11 &

```

```

&reg mat=1, cur=+22860& ; start of right-side top coil

```

```

&po x= 19.80,y= 18.11 &
&po x=  9.30,y= 18.11 &
&po x=  9.30,y=  5.31 &
&po x= 19.80,y=  5.31 &
&po x= 19.80,y= 18.11 &

```

```

&reg mat=1, cur=-22860& ; start of left-side bottom coil

```

```

&po x=-19.80,y=-18.11 &
&po x= -9.30,y=-18.11 &

```

```

&po x= -9.30,y= -5.31 &
&po x=-19.80,y= -5.31 &
&po x=-19.80,y=-18.11 &

&reg mat=1, cur=+22860& ; start of right-side bottom coil
&po x= 19.80,y=-18.11 &
&po x= 9.30,y=-18.11 &
&po x= 9.30,y= -5.31 &
&po x= 19.80,y= -5.31 &
&po x= 19.80,y=-18.11 &

```

The basic format of a region can be described by considering the section delineated as Region 1. This describes the total outline region used. Line 1 describes the region material as **mat=2** which is steel. As such for this problem, the material is assumed to be steel unless otherwise specified. The following five points describe the dimensions of the rectangular region. This list happens to begin in the bottom left corner of the rectangle, go up to the top left, across to the top right, down to the bottom right, and then back to bottom left. The starting point and order in which the points are described are arbitrary as long as each point has a coordinate in common with the point above it and a coordinate in common with the point below it (with exceptions for the first and last point which must always be identical.) As such, the general format for region points alternates between changing the x-coordinate and y-coordinate. White space is ignored by the compiler, so while the points have been formatted to improve readability, the exact spacing used is not essential. All geometry regions utilize this same point-by-point format to outline the shape, although headers may vary. The value **mat=1** is for air, and a current density can be specified for an air region using **cur=+22860** where a positive current density points into the page and a negative current density points out of the page.

To calculate a geometry file (for Windows):

This describes how to take a PSF geometry file and use the program Poisson to calculate the magnetic field.

Double click on the .am geometry file to run AUTOMESH.EXE. This produces a “.T35” file of the same name and files called “OUTAUT.TXT” and “TAPE35.INF”. These are the Poisson Superfish solution file, problem description file, and setup information files respectively.

1. Double click on the .T35 file to open it in the PSF plotting program (WFPLLOT.EXE). This will display the material and mesh region boundaries as specified in the geometry file (Figure 36).

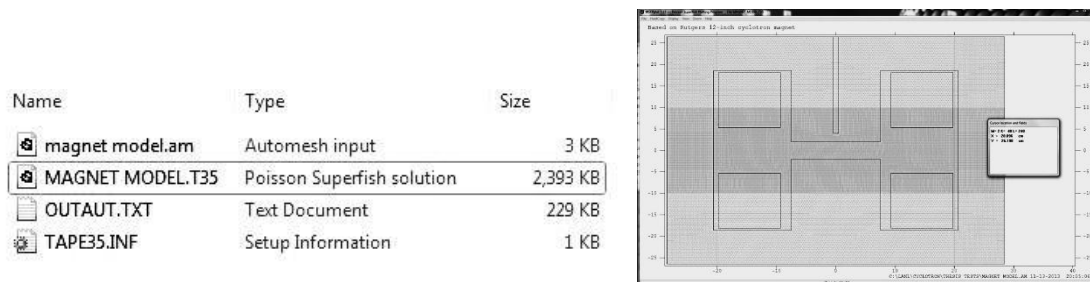


Figure 36: Files and plot after Automesh execution.

2. Right click on the .T35 file and choose “Run Poisson” to calculate the magnetic field. To view the plot with the magnetic field lines, the plot can be updated using Display → Redraw Plot or just closed and reopened.

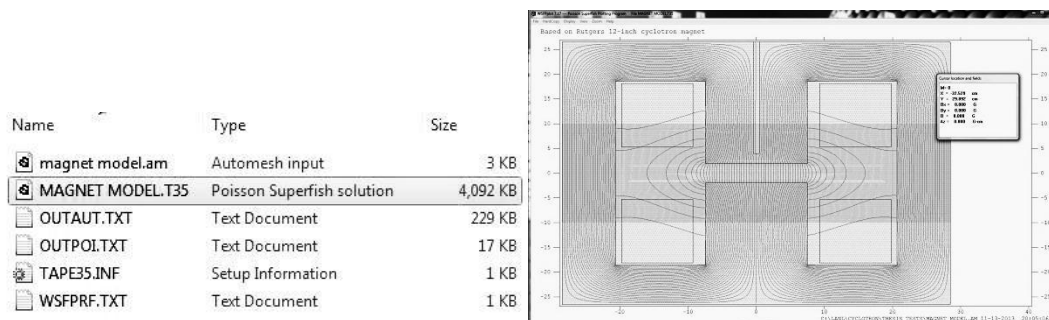


Figure 37: Files and plot after Poisson execution.

A.2 PSF to SIMION

To use a PSF magnetic field calculation as the magnetic field in SIMION 8.1, it is necessary to follow specific steps for exporting the magnetic field solution. The following steps and values are required to export the magnetic field for use with the SIMION 8.1 geometry ion bench made for the Rutgers cyclotron. If the Houghton cyclotron geometry is modelled, the specific values used may vary.

1. Right click on the .T35 file and choose “Interpolate (SF7)”.
2. Select “grid” and enter the variable values $X1=0$, $Y1=-2.5$, $X2=14$, $Y2=2.5$, X steps=140, and Y steps=50. These values are determined by the number of mesh points SIMION is expecting.
3. To export this file, click “Run”; this creates a file called “OUTSF7.TXT” which contains the calculated value of B_x , B_y , $|B|$, A_z , dB_y/dy , dB_y/dx , and dB_x/dy for each X,Y coordinate.

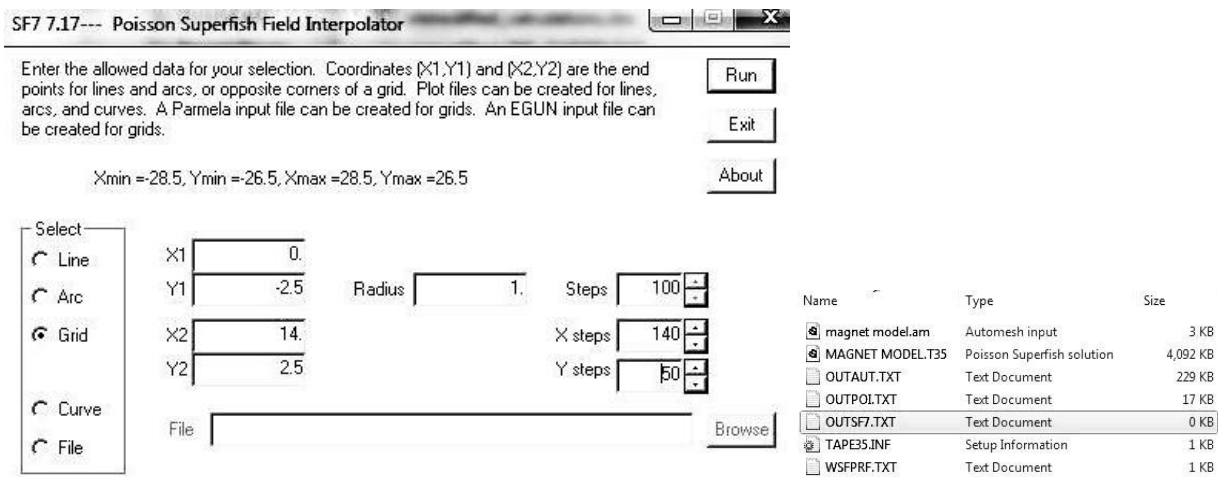


Figure 38: Interpolator window and files after interpolator execution.

4. Create a directory in C:\ called “PSF_2_SIMION” and copy OUTSF7.TXT into the directory. Open “PSF2SIMION.xls”. (Note: This is a spreadsheet created by Dr. Koeth which contains a macro to sort the data. A copy of this file should always exist in the folder “Rutgers’ Model Files – Do Not Change”, a subdirectory of the main Cyclotron directory. It does not matter

where this file is opened from, and it is convenient to keep a copy of PSF2SIMION.xls in the PSF_2_SIMION directory.)

5. Under the “Developer” tab in Excel (which may need to be added via “Options”/”Customize Ribbon”/Check “Developer (Custom)” under “Main Tabs”) click “Macros”, choose “Macro2”, and click “Run”. This sorts the OUTSF7.TXT into the format required for SIMION 8.1 and saves this file as “OUTSF7.csv” in PSF_2_SIMION.
6. Appendix B explains the setup process of SIMION 8.1. Assuming this has been completed, copy OUTSF7.csv into the working directory created in the “mystuff” folder in the SIMION 8.1 program files directory. The SIMION 8.1 file, “field_array.lua” created for the Rutgers cyclotron looks for a magnetic field file named “997Tesla2.csv”, so either change OUTSF7.csv to this name, or alter the .lua file.

The following link to the SIMION website offers a more in depth explanation to some parts of this process; however, the conversion method described above is a significant simplification made possible by using the SIMION ion bench created for the Rutgers cyclotron. This link also includes a number of other instructions for using PSF with SIMION: http://simion.com/info/poisson_superfish.html

A.3 PSF General Analysis

The export settings described in Section A.2 are specifically for use with the Rutgers’ setup in SIMION 8.1. Here is a general explanation of what these variables mean as for analysis of the PSF calculations it is often convenient to use different export settings.

In the grid option of the Interpolator as seen in Figure 38 the bounds are in centimeters, and the number of steps is the number of divisions in that range (such that the step size is $(X_2 - X_1)/X_{step}$). That is, for $X_1=0$, $X_2=14$, and $X_{steps}=140$, the Interpolator exports the magnetic field from 0cm to 14 cm making the range 14 cm which is then divided into 140 steps, so the X step size is 1 mm.

In general, to use the OUTSF7.TXT file the Interpolator produces, open Microsoft Excel, click “Open”, find the file (change the files it displays to “All Files”), and open it. (Note that it is important to open it this way. Right clicking on the OUTSF7.TXT and choosing open in Excel does not send the file through the Text Import Wizard which delimits the data.) In the Text Import Wizard choose “Delimited” in the first step, “Space” in the second step, and “General” in the final step.

For an analysis of the PSF magnetic field calculation along the central plane, it is convenient to use an Excel macro I made. I modelled it after the Rutgers PSF2SIMION setup described in Section A.2, so follow these steps with the following adaption: use the Interpolator values $X1=0$, $Y1=-0.2$, $X2=14$, $Y2=0.2$, X steps=140, and Y steps=10 (still in grid); create a directory in C:\ called “PSF_2_EXCEL” and copy OUTSF7.TXT into the directory. Open “PSF2EXCEL.xls” and run the macro called “Analyze_BField”.

Appendix B

SIMION 8.1

SIMION 8.1 is a software package designed to calculate electric fields and charge trajectories in three-dimensional static or radio-frequency systems.

Upon purchase, SIMION must be registered and downloaded at simion.com/u/register. When license information is entered, a license key called “simion.key” can be downloaded. Note that if SIMION license information is updated and a new license key is downloaded, it is essential to delete the old license key. Some SIMION features will write-out to the SIMION program directory so, if it is not implemented automatically, it may be necessary to manually allow these features. For Windows 7, this can be done by right-clicking on the program files directory for SIMION, choosing “Properties” and then under the “Security” tab choosing “Allow Modify & Full Control”.

B.1 Rutgers Setup

An ion workbench – a user-created program which can be opened in SIMION and configured to access a set of potential arrays – was created for the Rutgers cyclotron. This study has utilized this workbench for its calculations. In order to configure SIMION to access the Rutgers ion workbench:

1. Copy the following files from the directory of Rutgers files into the working SIMION directory (created somewhere in the “mystuff” folder in the SIMION program files):
“field_array.fly2”, “field_array.iob”, “field_array.lua”, “magnet.PA”,
“March_6_2013_proton_example.fly2”, “straightedgeD.PA0”, “straightedgeD.PA1”, and
“straightedgeD.PA2”.
2. Copy the magnetic field file into the working SIMION directory. Section A.2 describes how to create the magnetic field file. Rename the magnetic field file “997Tesla2.csv”.

3. Open SIMION, click “View/Load Workbench”, and choose the file “field_array.iob” that was placed in the working directory. This opens the ion workbench with the Dee potential arrays, a proton at the center in the Dee gap, and the magnetic field specified.
4. In the “Variables” tab specify values of “omega” (resonance frequency for the system in rad/ μ s) and “rf_voltage” (voltage amplitude, not peak-to-peak.) Note it is often useful for diagnostics to use a higher rf_voltage than the actual cyclotron (which uses rf_voltage=1500 V because it is 3000 V peak-to-peak.) In the “Particles” tab change “T.Qual” to 105 or greater. “SIMION_Calculations.xlsx” is set up to calculate omega using the maximum magnitude of the magnetic field. This value can be by opening the .T35 PSF file that plots the magnetic field and hovering over the area of interest (and reading the magnetic field in the dialogue box); alternatively, open the OUTSF7.TXT export file from PSF, find the value of Y that is closest to 0, and use the magnetic field strength for the corresponding X=0.
5. Click “Fly’m”.

B.2 Data Recording

To export the kinematic information about the ion and/or the electric and magnetic fields at the corresponding times, and output file can be specified to record selected values.

1. In the “Particles” tab check “Record data” and click on “Data Recording...”
2. The specific parameters chosen will vary depending on the intended purpose of the output file. As an overview, the “What Data to Record” column determines which variables will be recorded; certain variables such as “Ion number” are not insightful if you are running with only one ion. The “When to Record This Data” column determines what triggers a write out. For the best resolution, choose “Ion’s Every Time Step”; however, this outputs a large quantity of data which is sometimes difficult to analyze in Microsoft Excel. Therefore, if what is being tested for can be observed, for example, just by looking at the particle every time it crosses $Y=0$, choose the “Crossing Plane $Y=?$ ” option and choose 0 (at the bottom of the

column). The “Format for Recorded Data” column sets the format of the output file. For analysis in Excel choose “Delimited”, any Delimiter type is fine as long as you Delimit by that Delimiter when you import into Excel. The “G” number format is most compact, but “F” or “E” will work too; similarly setting “Width” and “Precision” to 0 allows the program to control these variables as is best for the given geometry. In the “Output File” dialogue box enter the name output file name. Including the extension .txt in the file name is advised. Section 8.6 (starting on page 8-20) of the SIMION 8.1 manual describes each data recording feature.

3. Select “OK” to save the data recording settings. Every time “Fly’m” is selected, a output file with the specified name containing the calculated values of the specified parameters will be created. If a file with this name already exists in the directory, it will be overwritten.

References

-
- [1] E. O. Lawrence, *Nobel Lectures in Physics* (World Scientific Publishing Company, Singapore, 1998), Vol. 3, p. 430.
 - [2] P. G. Kruger and K. Green, Phys. Rev. **51**, 699 (1937).
 - [3] G. Ising, Ark. Mat. Astron. Fys. **18**, 1 (1924).
 - [4] E. O. Lawrence and M. Livingston, Phys. Rev. **40**, 19 (1932).
 - [5] E. D. Courant, M. Livingston, H. Snyder, and J. Blewett, Phys. Rev. **91**, 202 (1953).
 - [6] E. D. Courant, M. Livingston, and H. Snyder, Phys. Rev. **88**, 1190 (1952).
 - [7] E. Dorman and R. Emery, in the Proceedings of Cyclotrons, Vancouver, 2013 (pre-release).
 - [8] T. Baumann *et al.*, Nature, **449**, 1022 (2007).
 - [9] A. M. Rogers *et al.*, J. Phys. Conf. Ser. **312**, 1 (2011).
 - [10] T. L. Grimm *et al.* IEEE Trans. Appl. Supercond. **15**, 2393 (2005).
 - [11] J. R. Richardson, E. Blackmore, G. Dutto, C. Kost, G. Mackenzie, M. Craddock, IEEE. Trans. Nuc. Sci. **22**, 1402 (1975).
 - [12] M. K. Craddock, in the Proceedings of the Particle Accelerator Conference, San Francisco, 1991, p.57.
 - [13] M. Yuly, in the Proceedings of Cyclotrons, Vancouver, 2013, p.286.
 - [14] D. Haas, B.S. thesis, Houghton College, 2009.
 - [15] J. J. Welch, K. Bertsche, P. Friedman, D. Morris, and R. Muller, Lawrence Berkley Laboratory Report No. LBL-23323, 1987 (unpublished).
 - [16] T. Feder, Phys. Today. **57**, 30 (2004).
 - [17] T. W. Koeth, A. Rosenberg, J. Kruzler, T. Ponter, W. Schneider, and D. Hoffman, in the Proceedings of Cyclotrons, Vancouver, 2013, p.366.
 - [18] T. W. Koeth, Nucl. Instrum. Meth. Phys. Res. B. (submitted Aug. 2014).
 - [19] H. T. Baumgartner, in the Proceedings of Cyclotrons, Vancouver, 2013, p.302.
 - [20] F. A. Ward, Proc. Phys. Soc. **51**, 810 (1939).
 - [21] M. S. Livingston, Rev. Sci. Instrum. **7**, 55 (1936).
 - [22] D. Kerst and R. Serber, Phys. Rev. **60**, 53 (1941).
 - [23] R. R. Wilson, Phys. Rev. **53**, 408 (1938).

-
- [24] M. S. Livingston and J. P. Blewett, *Particle Accelerators*. (McGraw-Hill Book Company, New York, 1962).
- [25] D. I. Manura and D. Dahl, *SIMION Version 8.0/8.1 User Manual* (Scientific Instrument Services, New Jersey, 2011), Revision 5, covering Version 8.1.0.31.
- [26] T. Koeth, G. Hine, D. Hoffman, J. Krutzler, T. Ponter, A. Rosenberg, K. Ruisard, and W. Schneider (unpublished).